SOLVENT INDUCED MODIFICATIONS TO FIBER NANOSTRUCTURE AND MORPHOLOGY FOR 12HSA MOLECULAR GELS

By

JIE GAO

A thesis submitted to the Graduate School – New Brunswick

Rutgers, The State University of New Jersey

In partial fulfillment of the requirements

For the degree of

Master of Science

Graduate Program in Food Science

Written under the direction of

Dr. Michael A. Rogers

And approved by

_____

_____

_____

New Brunswick, New Jersey

January 2014

ABSTRACT OF THE THESIS

SOLVENT INDUCED MODIFICATIONS TO FIBER NANOSTRUCTURE AND MORPHOLOGY FOR 12HSA MOLECULAR GELS

By JIE GAO

Thesis Director:

Dr. Michael A. Rogers

Molecular organogels are thermo reversible quasi-solid materials, which are formed by low molecular weight organogelators (LMOGs) undergoing supramolecular aggregation via non-covalent interactions, forming a three-dimensional fibrillar network. Numerous applications of molecular organogels are been investigated as edible oils, drug release matrices and personal care products.

The chemistry of the organic phase (i.e., solvent) influences every level of structure in organogels. Different solvents induce LMOG to assemble into “crystal like” fibers, which have more than one crystal form, lamellar arrangement and domain size. Differences in these solid states are known to affect the macroscopic properties of the gel, including critical gelator concentration (CGC), melting point, melting enthalpy and opacity.12-hydroxystearic acid (12HSA) was examined in several classes of organic solvents with different function groups. These gels, sols or precipitates were analyzed

using a series of techniques including: powder x-ray diffraction (XRD), differential scanning calorimetry (DSC), fourier-transform infrared spectroscopy (FT-IR), pulsed nuclear magnetic resonance spectroscopy (pNMR) and microscopy.

Specifically, certain solvents caused 12HSA to self-assemble into a triclinic parallel polymorphic form with subcell spacing of ~4.6, 3.9, and 3.8 Å and an interdigitated unit cell with a lamellar arrangement (38~44 Å). This polymorphic form corresponded to a less effective sphereultic supramolecular crystalline network, which immobilizes solvents at CGC greater than 1.5 wt %. The other group of solvents induce a hexagonal subcell spacing (i.e., unit sub cell spacing ~4.1 Å) and are arranged in a multi lamellar fashion with a unit cell greater than the bimolecular length of 12HSA (~54 Å).This polymorphic form corresponds to fibrillar aggregates with a CGC less than 1 wt %.

This thesis is dedicated to:

My parents

Tao Gao & Luya Wang

ACKNOWLEDGEMENTS

I would like to take this opportunity to express my sincerest gratitude to all the individuals who have made contributions to different aspects of my life during my studies. Their efforts have made it possible for me to commence and complete this great work. Despite many unpredictable difficulties and predicament I faced, their ongoing positive attitudes and supports encouraged me and allowed me to accomplish my studies.

The last two years of the thesis research has been exciting and nutritious for me. Firstly, I am deeply grateful to my Graduate Advisor: Dr. Michael A. Rogers for patiently taking me through this challenging academic journey. Without his contribution and involvement, the work could not be possible. He invested time and effort in the development of the thesis topic, literature collection, and the structure layout of the final thesis. I am amazed at his patience, which encouraged me when I was depressed in the midst of a vast ocean of academic difficulty. Dr. Rogers is a great mentor; many of the ideas would not have been realized without his help and the intense discussions.

I am also deeply indebted to Dr. Thomas J. Emge, the Chief Crystallographic Engineer in Wright-Rieman Laboratories. He not only offered X-ray equipment support, but also taught me the required operational and analytical skills. His contributions prompted me to successfully complete my experiment section of the study. I would also like to thank my project partner Songwei Wu for her collaborations while working in the huge project. It was enjoyable experience working with her. The discussions between us, while standing by the street for two hours, brought better understanding and inspiration on our research projects.

Most importantly, I want to thank my family: especially my parents for working their best to pay for my education, the opportunities and freedom to pursue my dreams and interests. When I was an undergraduate student in college, I was always wanting to study abroad to receive higher education in the United States to broaden my horizons. My parents never said “no” in terms of this situation and stood firmly and clearly to support me in the preparation of application for a graduate school. During my stay at Rutgers, a continuous stream of concerns was sent from the other side of Pacific Ocean. I truly felt their warmth and strength. Last but not least, I also would like to devote my special gratitude to my fiancé, Letian, for his selfless understanding and company. He has used his knowledge and experience to educate me in my daily life as well as study and work. He has dissolved my worries and confusions in many cases and brought me joy and peace beyond words and knowledge. We will step into a new phase in our life; I am deeply indebted to him for his love through this period and for many years to come.

PREFACE

The work presented in this thesis was conducted in the Department of Food Science, School of Environmental and Biological Sciences, Rutgers, The State University of New Jersey and the Department of Chemistry and Chemical Biology, Rutgers University, The State University of New Jersey. It is a result of my work during the period between September 2011 and December 2013.

Chapter three and chapter four of this thesis are co-authored by Dr. Michael A. Rogers. With pride, chapter three has been published in *Crystal Growth & Design:* entitled "Solvent-Induced Polymorphic Nanoscale Transitions for 12-Hydroxyoctadecanoic Acid Molecular Gels", (DOI10.1021/cg400124e), Received: January 22, 2013 / Published: February 5, 2013. Chapter four has been published in *CrystEngComm:* entitled "Nanoscale and Microscale Structural Changes Alter the Critical Gelator Concentration of Self-assembled Fibrillar Networks", (DOI 10.1039/C3CE40323H), Received: 21 February 2013 / Accepted: 22 April 2013/ Published: 22 April 2013.

Table of Contents

List of Figures

List of Tables

List of Appendices

1.0 Introduction

Lipids are differentiated from other macronutrients based on their solubility in organic solvents and insolubility in water. More specifically, lipids contain one, two, or three fatty acids esterified to glycerol [1]. Lipids are typically sub-categorized as either saturated or unsaturated fatty acids [1]. Saturated fats are triglycerides containing only fully saturated carbon atoms (i.e., there are no double bonds present on the fatty acids). Conversely, unsaturated fats are lipids that have one or more double bonds between their carbon atoms. Unsaturated fats are further classified as either *cis or trans* unsaturated. The *cis* isomer is commonly present in nature; while *trans* fats, are typically formed during food processing and biohydrogentation in rumen animals [2], [3].

In food manufacturing, both saturated and unsaturated fats are commonly used for many reasons [4]. Saturated and unsaturated fats are able to provide important structural elements to lipid based food product; saturated fats typically provide the elastic properties while unsaturated oils provide the viscous properties [5], [6], [7]. They also improve the texture, appearance, lubricity, mouth feel and flavor of food product, contributing to their palatability [8]. Although the structures and flavor are desirable, saturated fats and *trans* fats, a subcategory of unsaturated fats, have been shown to have deleterious influence on human health [9].

During digestion, approximately 95 % of the fat in food is digested and absorbed [10]. Further, saturated fats have been shown to raise total cholesterol and low-density lipoprotein (LDL) cholesterol levels, which are risk factor for cardiovascular disease [11]. *Trans* fats not only increase unhealthy LDL cholesterol but also lower healthy high-density lipoprotein (HDL) cholesterol [3], [12], [13], [14], [15]. In general, consumers

should reduce their consumption of saturated and *trans* unsaturated fats; however, their physical elastic properties cannot be replaced and hence are difficult to eliminate from numerous manufactured foods. Therefore, it is critical to find alternatives to hardstock fats (i.e., saturated and *trans* unsaturated fats).

One possible strategy is to replace hardstock fats using unsaturated oils and to provide the elastic component with a molecular gel. Molecular gels are formed using low molecular weight organogelators (LMOGs) dispersed in an organic phase such as vegetable oil [16], [17]. Pernetti et al., have proposed structuring edible oils with LMOGs to reduce saturated fats, using single and/or mixed gels [18]. Organogels formed using LMOGs have also attracted considerable attention in the pharmaceutical and petrochemical fields [19], [20]. For instance, organogels with glyceryl fatty acid ester gelators have been shown to enhance dermal permeation during topical drug delivery [21].

Although molecular gels have been widely study, the effect of solvent on self-assembly of LMOGs into self-assembled fibrillar networks (SAFiNs) has been overlooked. Gelation using LMOGs results in the formation of a three-dimensional network structured via non-covalent intermolecular interactions [22]. The “crystal-like” properties of SAFiNs have been shown to exist in more than one crystal polymorphic form depending on the solvent characteristics. The lamellar arrangement as well as the domain size vary as a function of solubility parameters [23], [24]. Different solid states are known to affect the macroscopic properties including: critical gelation concentration, melting point, melting enthalpy and opacity of the gel [25]. Those physical properties are essential if organogels are to be used as alternative for hardstock fat.

12-Hydroxystearic acid (12HSA) is an extremely effective simple organogelator derived from hydrogenated castor seed oil which has the ability to gel a variety of organic solvents [26], [27]. Although it is not currently food grade it provides an ideal system to study the effect of solvents due to its fatty acid properties [27]. To better understand the impact of solvent on the assembly of 12HSA we will examine the effect of different organic solvents with varied function groups and aliphatic chain lengths to study the nanostructure and microstructure of the molecular gels.

2.0 Literature Review

2.1 Organogels

Organogels are distinguished from hydrogels based on their liquid phase. Before broadly discussing the formation mechanism of organogels, we need first to define a gel. The scientific term was first presented in literature by Thomas Graham in 1861and he relied on a macroscopic observation of silica acid gels and postulated that the aggregation form is a colloidal condition of matter [28]. 65 years later, a prophetic statement "[....] the colloid condition, the gel, is easier to recognize than to define" was proposed by Dr. Dorothy Jordan Lloyd [29].After that, various definitions evolved. Hermans defined a gel by connecting macroscopic and microscopic properties together suggesting that the coherent colloid dispersed system must contain at least two components and exhibit solid like mechanical properties; and both the dispersed (gelator) phase and dispersion medium extend continuously throughout the system [30]. Most recently, Weiss and Terech provided the most elaborate and comprehensive definition, which is a gel must contain two features: 1) a continuous microscopic structure with macroscopic dimensions that is permanent on the time scale of an analytical experiment; and, 2) is solid-like in its rheological behavior, despite being comprised mostly of liquid [31].

Organogels are subdivided into two categories based on the mechanism of gelation including: chemical polymerization and physical self-assembly [32], [33]. In chemical polymerization, polymer chains, with various reactive sites, are covalently linked forming a 3D network in the presence of cross-linker, leading to the formation of a thermally irreversible network [32], [34]. Physical self-assembly relies on LMOG to assemble via non-covalent interactions thereby immobilizing the organic solvent within

the network of fibers, rods, liquid crystals, micelles or ribbons[35]. The self-assembled networks creates a 3D network immobilizing organic solvent by weak inter-chain interactions such as hydrogen bonding [33], [36], [37], [38], van der Waals interactions [39] and π-π stacking [40]. Hence, physical gels are thermally reversible and exhibits a 'gel-like' rheological property [31].

Two factors affect the gelation process in LMOGs; the first is the molecular structures of organogelator [41] and the second is the properties of solvent [33]. In molecular gels, the LMOG undergoes spontaneous formation into a SAFiN and the fibers are entangled with each other, resulting in a 3D network [42]. LMOGs can be as simple as n-alkenes [43] relying solely on London dispersion forces/van der Waals interactions [24]. As the molecular complexity increases so does the molecular interactions which stabilize in SAFiNs. As an example, if a n-alkane is has a methyl group replaced with a carboxylic acid moiety it provides additional intermolecular interactions (such as hydrogen bond) for network formation [24]. Furthermore, the properties of the medium such as solubility and LMOG-solvent interactions alter the gelation process [33], [41]. The solubility of the LMOG in certain solvents depends on the polarity of the solvent which is effected by the function groups present, which in turn effects the critical gelator concentration (CGC) [33]. Gelators that have high solubility will lead to strong gelator-solvent interactions promoting dissolution [44]. Conversely, LMOGs that have a low solubility have weak gelator-solvent interactions and as such gelator-gelator interactions are favored potentially leading to gelation.

2.2 Molecular Gels

In molecular gels, LMOGs self-assemble into supramolecular aggregates forming a SAFiN at low concentrations (< 2 wt%) when a solution or sol is cooled [31]. Gel formation occurs via a multi-step process. First, the gelator must be dissolved in an organic solvent by elevating the temperature resulting in a sol [31]. Upon cooling below the gelators characteristic gelation temperature (T_{gel}), the solution becomes super-saturated causing microscopic phases separation rather than the macroscopic separation typically occurring in 3D crystallization processes [31]. Instead, gelator molecules self-assemble in stochastic nucleation events which have highly specific interactions allowing preferential 1D growth [31]. One-dimensional crystal growth promotes the formation of fibers, rods, liquid crystals, micelles or ribbons which have large aspect ratios [23].

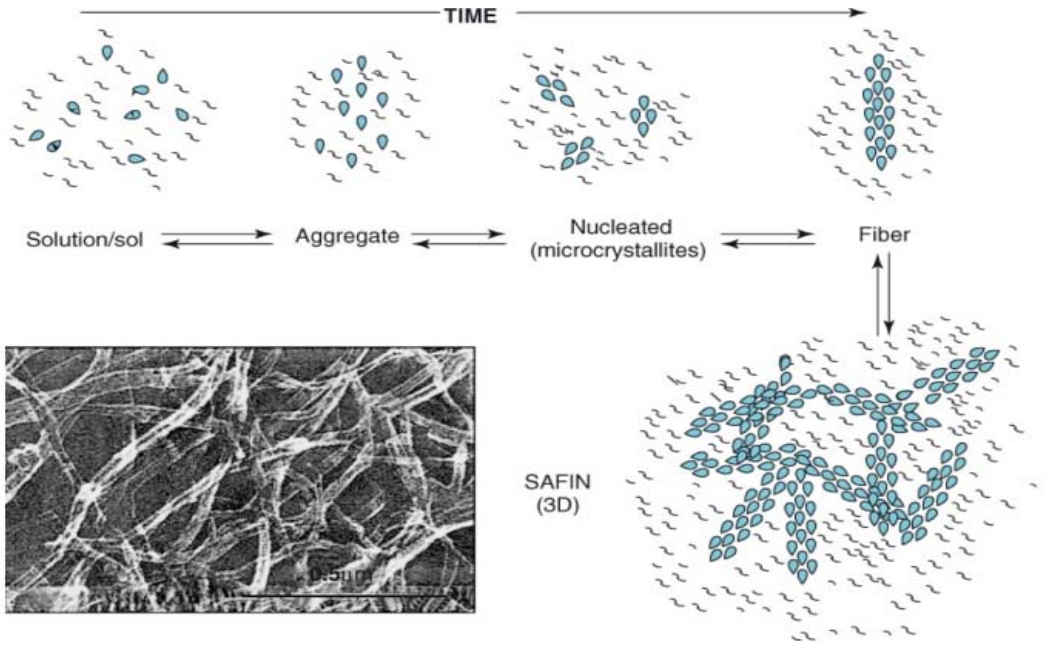

Figure 2-1: Schematic representation of the formation of a 3D SAFiN formation beginning from the sol [44].

2.3 SAFiN Gelation

Self-assembly of LMOGs is a balance between solubility and aggregate in solvents [44]. SAFiNs occur when the gelator molecules perform supramolecular aggregation via weak non-covalent inter-molecular interactions, including hydrogen bonding [33], [36], [37], [38], van der Waals forces [39] and π-π stacking [40]. Upon cooling from a sol three possible scenarios occur: 1) the gelator molecules form highly ordered 3D crystals which precipitate out of solution[44], 2) the gelator molecules can precipitate due to random amorphous aggregation[44], and 3) the gelator molecules self-assemble with highly specific interactions promoting 1D growth [31]. These 1D aggregates interact with one-and-other to form a 3D fibrillar network described as 'crystal-like' [22].

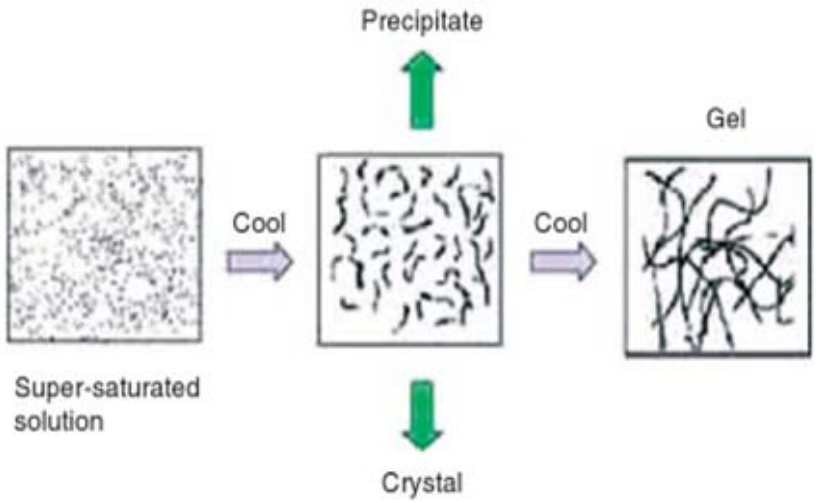

Figure 2-2: Schematic representation of aggregation modes [44].

2.3.1 Structure Levels of SAFiN Gelation

SAFiNs have multiple levels of structure ranging from the nanoscale to the macroscopic scale [45]. The primary structure is the structure from the angstrom to

nanometer scale and is often referred to as the polymorphic form and domain structure [44]. LMOGs interact via non-covalent bonds, leading to the formation of arrays and lamellar structures which serve as platforms for the following formation of rods, tubes or sheets (primary structure) [44]. Commonly, hydrogen bonding drives the formation of the primary structure [33],[36],[37],[38],[44]. For instance, 12HSA forms molecular gels via the dimerization of carboxylic acid head groups and then form a secondary hydroxyl hydrogen bond from the alcohol groups on the fatty acid backbone.

The secondary structure is the 3D network of the rods, tubes or sheets [32].

The tertiary structure occurs from the micro- to macro- scale and involves 3D supramolecular arrangement [44]. For instance, short, rigid fibers are less effective than long, flexible fibers at immobilizing solvent [45]. This level of structure determines the macroscopic properties of the material such as hardness and elasticity [45].

2.3.2 Crystallographic Mismatch Branching Theory

It is generally confirmed that SAFiNs are a result of a nucleation-growth-mismatch process that consists of primary nucleation and subsequent growth and branching of fibers [31]. Crystallographic mismatch branching (CMB) theory explains that branching occurs at the tip or side faces of growing fibers. Similar to crystal nucleation and growth, the kinetics of CMB depend on the degree of supersaturation at the surface of the growing crystal [38]. At low degrees of supersaturation, the crystallographic mismatch nucleation barrier (ΔG^*) is high, favoring fiber growth without branching (Figure 2-3 a) [46], [47]. As the degree of supersaturation increases, the ΔG^* will decrease, and interfacial structural mismatches cause molecules to adhere to

the growing interfacing without optimal orientation leading to a branch point at the surface of the parent crystal (Figure 2-3 b) [37], [46], [47].

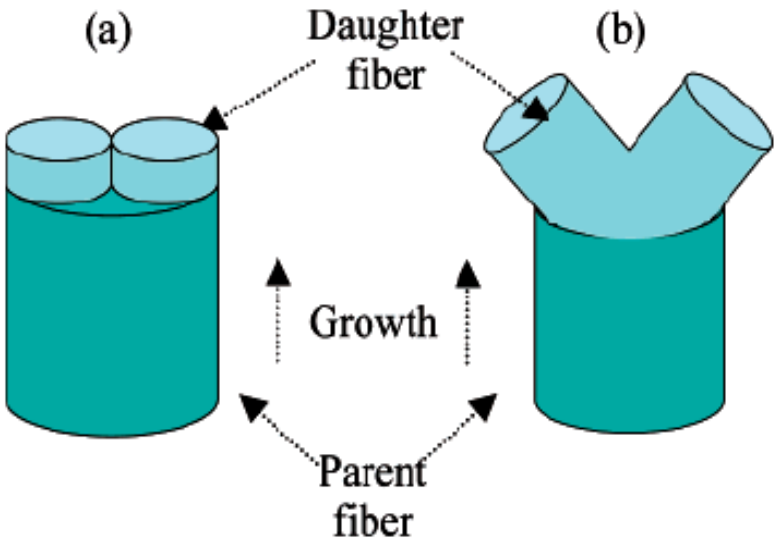

Figure 2-3: Schematic representation of CMB theory: (a) the formation of elongated fibers due to a perfect structural match (b) crystallographic mismatch at the surface of fiber [38].

Recent work by Liu et al., has used CMB theory to model fiber branching in molecule gels (Figure 2-4) [46], [48]. Crystal growth commences from the surface of the nucleation sites. If it is under low-supersaturation conditions, crystal growth with fewer-branched fibers occurs. Those fibers entangle forming an interconnected fibrillar network [46], [48]. Under degrees of high-supersaturation, SAFiN growth is disrupted by mismatches and forms highly branched fibers that are usually short and thin resulting in a space-filling network structure (i.e., a spherulitic network) [46].

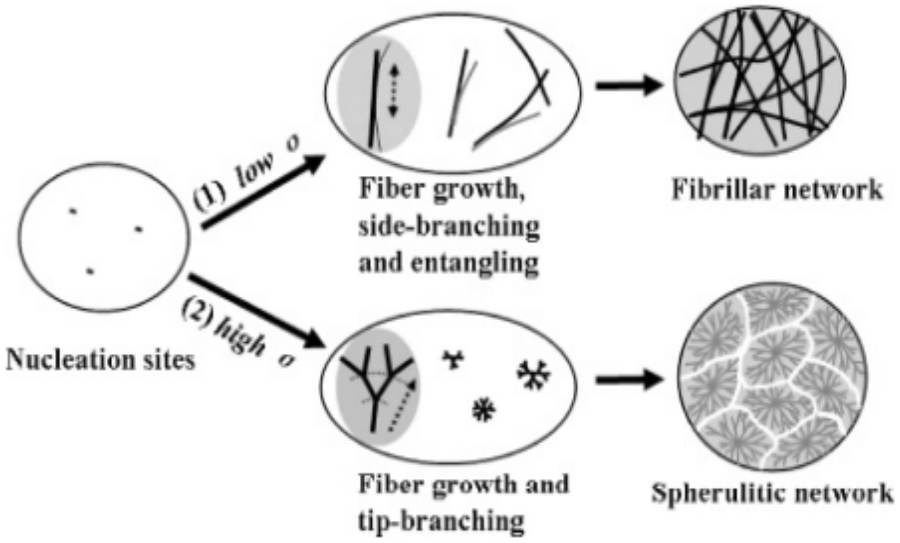

Figure 2-4: Two growth models for the formation of SAFiNs. (1) Under low degree of supersaturation and (2) under high degree of supersaturation [46].

2.3.3 Junction Zones

In SAFiNs there are two types of junctions zones -- transient and permanent [36][49][45][46]. Transient junctions are entangled fibers that exhibit very little elasticity over long ranges[36]. Permanent junction zones occur as a result CMBs at the surface of the crystal [45], which is controlled by super saturation[46].

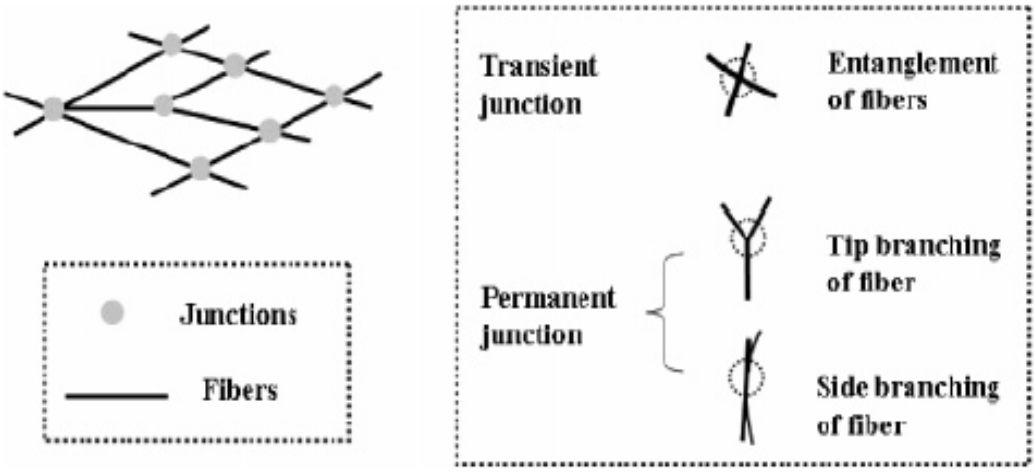

Figure 2-5: Schematic representation of the types of junction zones in SAFiNs [45].

2.4 Applications of Organogels

Numerous practical applications of organogels are being investigated by researchers including: crystalline fat alternatives in processed foods [18], drug delivery mediums for topical and oral pharmaceuticals [20], [42], and personal care products (i.e., shampoo, conditioner, soap, toothpaste, etc.) [50]. As reported, interest in organogels has rapidly grown in past decade [18], [20], [31], [51]. In food industry, hardstock fats may be replaced with vegetable oil based organogels [18]. Originally, the food industry was interested in 12HSA molecular gels to thicken peanut butter [52]. In pharma, organogels are being investigated as drug and vaccine delivery vesicles [19]. One of the advantages of organogels is that they have been shown to enhance permeation during topical drug delivery. For instance, sorbitan-based organogels, prepared by dissolving 20% sorbitan monostearate (SMS) in liquid surfactants (e.g., polysorbate 20 or 80), were tested and well-tolerated by volunteers [21]. Another example of an investigated drug delivery organogel is of piroxicam from an organogel composed of glyceryl fatty acid ester (GFAE) gelators in pharmaceutical oils [53]. The *in-vivo* skin penetration test showed superior uptake for the GFAE gelators compared to traditional formulations [54].

2.5 12-Hydroxystearic Acid

2.5.1 12HSA Lamellar Crystal Structure

12HSA has two functional groups: the carboxylic acid head group and hydroxyl group at position 12 [55]. The polar carboxylic acid head groups served as a hydrogen donor and acceptor forming a cyclic dimer in the lamellar structure [44], [56]. The secondary hydroxyl groups at position 12 forms hydroxyl hydrogen bonds with

neighboring molecules [23], [56]. After that, the hydrogen bond sequences occurs along the a axis (Figure 2-6) when 12HSA molecules stack to form the lamellar structure, which is the foundation for building primary structure of SAFiNs [49].

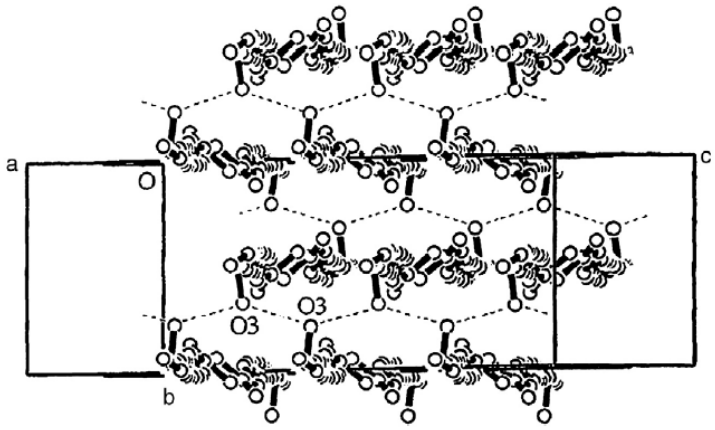

Figure 2-6: Crystal structure of 12HSA showing the hydrogen bond arrays [55].

Figure 2-6 shows the crystal structure of a 12HSA. Molecules stack to form a lamellar structure with the hydroxyl groups at position 12 forming a hydrogen bond sequence along the a-axis [55]. The distance between 12 hydroxyl groups is 2.87 Å and the angle at the C12-O3--O3 is 117 ° [55]. The twist pattern in 12HSA molecules is due to the hydrocarbon chains adopting an approximate all-trans configuration [55]. The angle of the fatty acid back-bone from C4-C5-C6-C7 and C15-C16-C17-C18 is 180°, while C10-C11-C12-C13 has a bond angle of 173° [55]. Dimers form between two carboxylic acid head groups and the distance between adjacent O2--O3 atoms is 2.62 Å [55].

2.5.2 Thermal Properties and Phase Behavior

The melting point of 12HSA is ~76 ^{o}C and a melting enthalpy of 182 kJ/kg [57]. The thermal properties of 12HSA in canola oil organogels illustrate that as the gelator

concentration increases, the melting enthalpy and the onset melting temperature increase, which is an indication of the amount of crystalline mass and crystal perfection in the gel [17]. The temperature in which crystallization occurs at also affects the melting enthalpy of 12HSA/canola oil gels. Rogers et al., [49] reported that as crystallization temperature increases, the melting enthalpy decreases, which may be due to a lower amount of crystalline material formed at high crystallization temperatures. This was later confirmed using both pulse-NMR and DSC measurements [49].

12HSA-canola oil organogels change as a function of time and storage temperature [58]. At high temperature, prolonged storage time results in a decrease in the melting enthalpy, which is an indication of less crystalline mass/order [59]. At low temperatures, the melting enthalpy continues to increase along with the storage time, which can be attributed to increased non-covalent interactions between fibers. Those interactions affect the total melting enthalpy without changing the crystalline mass [59]. Besides influencing the amount of crystalline material, the crystallization temperature also affects the crystalline packing of the 12HSA molecules within the gel [17]. The entropy of the gel, stored at high temperatures, remains constant but the entropy at low temperatures decreases in time [59].

2.6 Hansen Solubility Parameters

To better understand SAFiN formation, many attempts to correlate solvent parameters with gelation ability have been made [60], [61]. Hanabusa and Matsumoto first related gelation ability to a three component solubility parameter for various solvents and found that gelation abilities for cyclo(dipeptide)s are closely related to the polar component of the solubility parameters [62]. Several years later, Hirst and Smith tried to

use Kamlet-Taft hydrogen bonding parameters to predict the mesoscopic scale effects on gelation formation [63]. They observed solvents that possessed a low polar solubility parameter resulted in optically transparent, thermo reversible gels and as the polar solubility parameter increased, the gel strength weakened and eventually was no longer observed [63]. Before Hansen Solubility Parameters (HSP) are broadly discussed, the parameter should first be defined. Solubility parameters are derived from the cohesion energy parameters (i.e., the energy required to convert liquid to gas) [64]. All types of intermolecular non-covalent bonds that hold liquid molecules together must be broken before evaporation may occur, thus the cohesion energy is the direct measure of the energy of evaporation.

2.6.1 Hilderbrand Parameters

Hildebrand and Scott first defined the solubility term as the square root of the cohesive energy density, the heat of vaporization divided by the molar volume [65]:

$$\delta = (E / V)^{1/2} \quad (1)$$

where V is the molar volume of the pure solvent, and E is vaporization energy. HSPs are governed by the free energy of mixing the gelator and the solvent and free energy of mixing must be zero or negative so that the dissolution process occurs spontaneously [64]. The free energy change for a dissolution process is governed by [64]:

$$\Delta G_m = \Delta H_m - T\Delta S_m \quad (2)$$

where ΔG_m is the Gibbs free energy change during mixing, ΔH_m is the change in enthalpy during mixing, T is the absolute temperature and ΔS_m is the entropy change during mixing.

In polymer physics, it is assumed that the dissolution of the polymer is accompanied by a minor increase in the entropy, and the enthalpy is the deciding factor of the Gibbs free energy change [61]. Hildebrand and Scott derived the Hildebrand solubility parameter in two seminal papers to rely solely on the enthalpy [66]:

$$\Delta H_m = V\left(\left[\frac{\Delta E_1^v}{V_1}\right]^{1/2} - \left[\frac{\Delta E_2^v}{V_2}\right]^{1/2}\right)^2 \phi_1\phi_2 \tag{3}$$

where ϕ_1 and ϕ_2 are volume fraction of species 1 and 2 in the mixture. V is the volume of the mixture. ΔE_1^v and ΔE_2^v are the energy of vaporization of species 1 and 2 in the mixture, V_1 and V_2 are the molar volume of species 1 and 2 in the mixture.

2.6.2 Hansen Solubility Parameters

Based on the work of Hildebrand and Scott [66], Hansen proposed an extension of the Hildebrand parameter method to decompose the Hildebrand parameter into three components: (atomic) dispersion forces, (molecular) permanent dipole–dipole forces, and (molecular) hydrogen bonding (electron exchange) [64]. In other words, the total energy of vaporization for a liquid consists of several individual parts: dispersion, polar, and hydrogen bonding.

There are three major of interactions in organic materials [60], [61], [64], [67]. The first interaction is the dispersive interactions derived from atomic forces and typically are dominated by London dispersion forces and van der Waals interactions [64]. For the saturated aliphatic hydrocarbons, their energy of vaporization is comprised of only cohesive interactions (E_d) [61]. The second cohesion energy arises from the permanent dipole–dipole interactions (e.g., the polar cohesive energy (E_p)) [64]. Dipole-dipole interactions are attractive forces between the positive end of one polar molecule

and the negative end of another [64]. For example, saturated fatty acids constitute polar and dispersive components, so both dispersive and polar cohesive energy must be considered and calculated [61]. The third major cohesive energy component is the hydrogen bonding parameter (E_h) [64]. The basis of this type of cohesive energy is attraction among molecules because of the hydrogen bonds. In this simplified approach, the hydrogen bonding parameter has been used to more or less collect the energies from interactions not included in the other two parameters [64] .

The basic equation governing the HSPs is the sum of the individual total cohesion energy, E [64]:

$$E = E_d + E_p + E_h \quad (4)$$

Under isothermal vaporization of the saturated liquid, the cohesive energy density is the energy of vaporization per cm^3 which corresponds to the Hildebrand parameter. Dividing equation (4) by the molar volume (V) gives the square of the total (or Hildebrand) solubility parameter (δ) as the sum of the squares of the HSP d, p, and h components [64]:

$$E/V = E_d/V + E_p/V + E_h/V \quad (5)$$

$$\delta^2 = \delta^2_d + \delta^2_p + \delta^2_h \quad (6)$$

Recently，Raynal and Bouteiller performed a meta-analysis, applying the HSPs to numerous LMOGs to evaluate gelation behavior [60]. Their meta-analysis revealed that the solvents which gelled had similar HSP with only a few exceptions [60]. This promising tool was experimentally validated and predicted the gelation ability of 12HSA in numerous solvents [61]. It was determined that the ability of 12HSA to assembly in various solvents depended on the δ_h and was instrumental in defining if an opaque or

transparent clear gel formed or if it was a precipitate. As well, it was found that the CGC is linearly correlated with δ_h [61].

2.6.3 Hansen Space

Hansen space is the location of a molecule in 3D space comprised of the dispersive HSP, polar HSP, and hydrogen-bonding HSP parameters [68]. In Hansen space, molecules in close proximity to each other are soluble [68]. The distance between two molecules in Hansen space have a distance which is R_a, where [68]:

$$(R_a)^2 = 4(\delta_{d2} - \delta_{d1})^2 + (\delta_{p2} - \delta_{p1})^2 + (\delta_{h2} - \delta_{h1})^2 \quad (7)$$

The solvent HSPs fall in the solubility sphere indicates the bitumen is soluble; conversely the solvent HSPs distributed outside the solubility sphere means the bitumen is insoluble (Figure 2-7) [69]. Hansen space has also been mentioned by Raynal and Bouteiller [32] and Jie et al., [61]: If the solvent HSPs fall in the solubility sphere or in the gelation sphere, then this solvent is likely to dissolve or to be gelled by the LMWG.

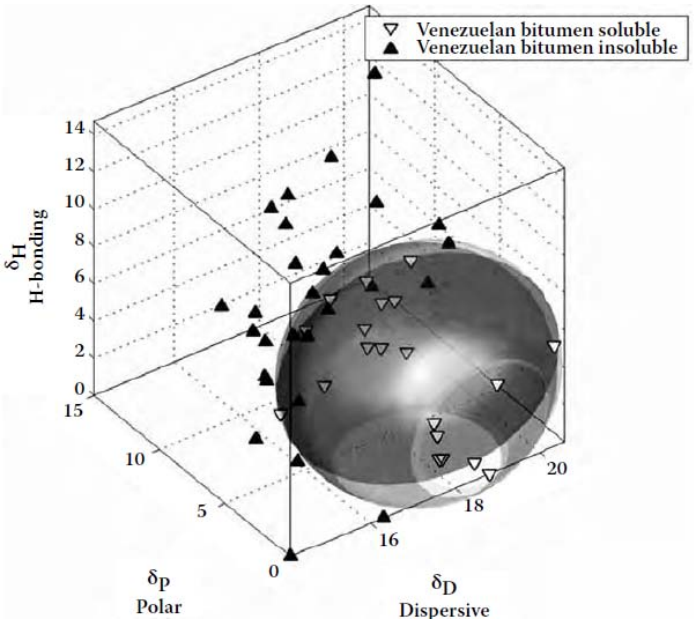

Figure 2-7: Hansen space of the selected solvents used for bitumen. The light-colored ellipsoid with largest volume is Hansen space [69].

2.7 Polymorphism

2.7.1 Polymorphism of Fatty Acids

Numerous compounds, including fats and molecular gels have numerous polymorphic forms which is the ability to configure to more than one crystal form [23], [25], [49], [56]. Solid state polymorphic forms are known to affect the macroscopic properties of the material, including its melting point and rheology parameters [70]. Fatty acid polymorphism was first presented by Duffy where three melting points for mutton and beef stearine were reported [71]. It was not until 81 years later that polymorphism was studied using powder X-ray diffraction (XRD) [72].

Polymorphs have different stabilities and unstable forms spontaneously change to more stable forms at ambient temperature (Ostwalds step rule) (Figure 2-8) [25][73]. Polymorphism, in fats and 12HSA, is a reflection of different molecular packings of the hydrocarbon chain [25]. Transformation of polymorphic forms can occur within the solid state or be melt-mediated. α, β', β can all form directly from melt. The α form is the most unstable form among the three, thus it may transform into more stable forms including β' and β. Soild state recrystallization can only occur in the direction from lower stability to higher.

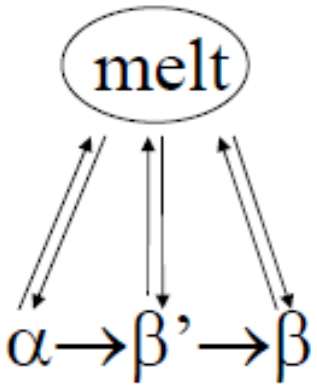

Figure 2-8: Illustration of Ostwalds step rule for the dynamics of polymorphic crystallization and recrystallization in fats [25].

2.7.2 Subcell and Subcell Packing

The simplest repeating unit in a crystal is the unit cell while the smallest spatial unit along the chain axis is the subcell (Figure 2-9). When fatty acids are analyzed using powder x-ray diffraction (XRD), two spacing are observed and associated with unit cell (long spacing or small angle spacing) and subcell (short spacing or wide angle spacing)[74].

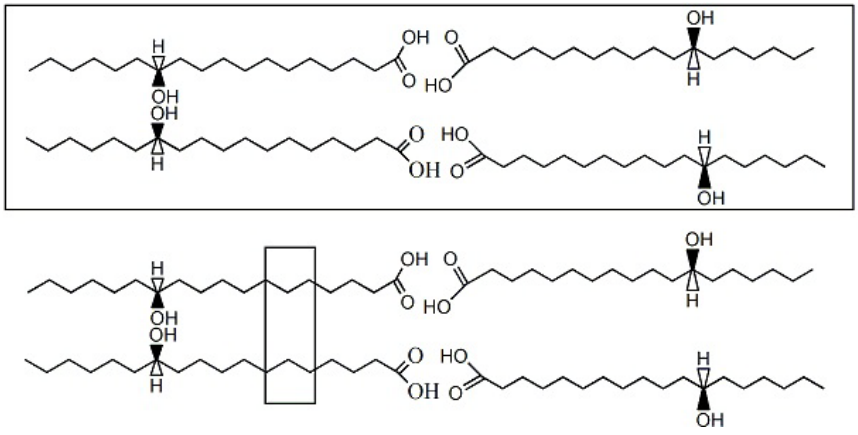

Figure 2-9: Diagram depicting the unit cell (Top box) and the subcell (Bottom box) for 12HSA.

XRD measurements can not only determine the polymorphic form but can also measure the domain thickness (i.e., number of molecular layers in a crystal)[24]. Three

main chain packing arrangement(in the case of fatty acids it is the methylene groups) are the [25]: hexagonal (α), triclinic (β) and orthorhombic (β') subcells (Figure 2-10). The α polymorphic form is characterized by a short spacing at 4.15 Å[75]; β' has two short spacings at 3.8 Å and 4.2 Å[76], and β has a short spacing at 4.6 Å[75].

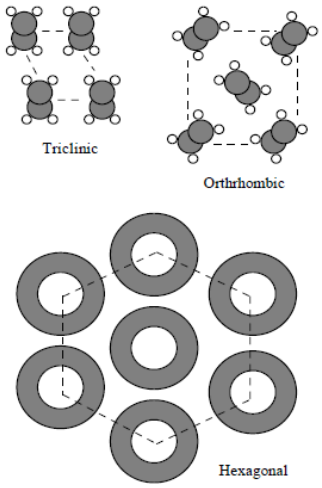

Figure 2-10: Molecular models of geometric packing arrangements of the sub cell packing for the hydrocarbon chain in the fatty acid backbone [26].

2.8 Methods of Structural Analysis for Organogels

2.8.1 Powder X-ray Diffraction

XRD is used to determine the organogel nanostructure using high energy light [77].X-rays are diffracted at specific angels caused by zones of constructive and deconstructive interference. This pattern of constructive and deconstructive interference provides information on the spacings between layers and rows of atoms; the orientation of fibers in SAFiNs and the size and shape of the crystalline region [77].

Diffraction patterns are described using Bragg's law where the distance between two waves is x, or $2d\sin\theta$, d is spacing between layers and θ is scattering angle [78].

When the path difference is equal to an integral number of wavelengths, constructive interference will occur and leads to Bragg's law:

$$n\lambda = 2d\sin\theta \tag{8}$$

where n is an integer of the higher order reflections and λ is the wavelength.

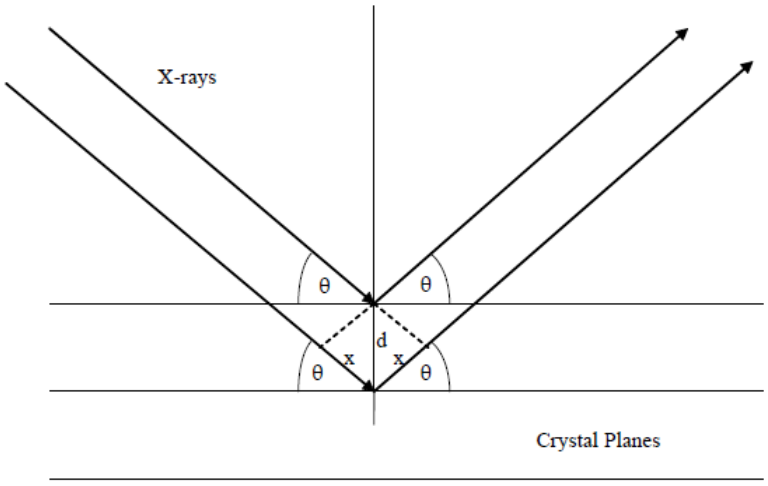

Figure 2-11: Geometry of the refection of x-rays from crystal planes used in the derivation of Bragg's law [25].

2.8.2 Differential Scanning Calorimetry

Differential Scanning Calorimetry (DSC) is a thermal technique that measures the temperature and heat flow associated with transitions in materials as a function of cooling rate [79]. These measurements provide information about physiochemical changes that involve endothermic or exothermic processes [79]. When the sample undergoes a phase transitions, more or less heat is needed to maintain both sample and reference pans at the same temperature, which leads to a differential temperature (ΔT) [73]. By observing the difference in heat flow between the sample and reference, DSC measures the amount of heat absorbed or released during phase transitions [73].

2.8.3 Pulsed Nuclear Magnetic Resonance Spectroscopy

Determination of the solid (often used for fats) content (SFC) using pulsed nuclear magnetic resonance spectroscopy (p-NMR) is more accurate than DSC. pNMR determines the rate of magnetism (alignment to the permanent magnate)of hydrogen nuclei. Free Induction Decay (FID) or nuclear relaxation differentiates solid phase relaxations from liquid relaxations [80]. When more than one component (i.e., a solid or gel and a liquid) is present, the magnetization decay corresponding to each component relaxes at different rates (Figure 2-12) [73]. There is a sharp magnetization decay initially at~10 μs, which corresponds to the solids [73]. The sharp initial decay is followed by a second slower decay which corresponds to the liquid component [73].

T_A is the decay time which describes the exponential decay corresponding to the transverse magnetization return to equilibrium [81]. T_A relaxations, below 70 μs, are proportional to the perfection of the crystalline phase [82].

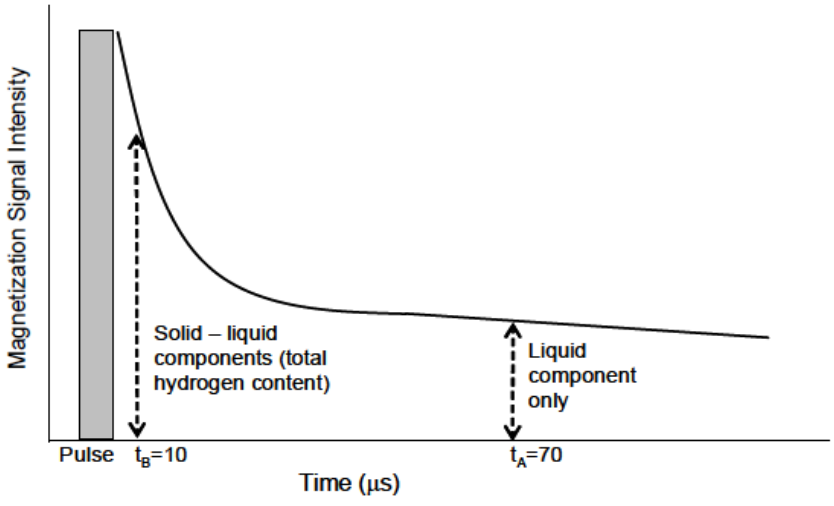

Figure 2-12: Magnetization decay of a sample used to determination the solid content by p-NMR [25].

2.8.4 Fourier Transform Infrared Spectroscopy

Fourier transform infrared spectroscopy (FTIR) utilizes the vibrational and rotational energies of different functional groups to identify the structural and chemical state of functional groups[83]. Of particular interest is the hydroxyl (O-H) and carboxylic acid (COOH) stretching frequencies that fall in the range of 3600-3200 cm^{-1} and 1700cm^{-1},the C-H stretching occurs between 3300 to 2800 cm^{-1}[83]. The chemical environment has a large effect on the energy associated with the different functional groups. For example, hydrogen bonding has a significant influence on the peak shape and intensity, usually causing peak broadening and shifts to lower frequencies as it forms non-covalent intermolecular bonds [24].

2.9 Objectives

Although numerous studies have been conducted on organogels and a general understanding of how these molecular assemble; many critical questions remain unanswered. Herein, the objectives of this research are:

1) *To examine 12HSA in numerous solvents which have different functional groups and aliphatic chain lengths to study the solvent effects on the nanostructure and microstructure of the molecular gels.*

2) *To study the nanostructure and microstructure of the gels in different solvents with concentrations varying between 0.2 to 2.5 wt%.*

2.10 Works Cited

[1] Nawar, W.W., *Lipids*, in *Food Chemistry*, O. R. Fennema, Editor. 1996, Marcel Dekker: New York . p. 225–320.

[2] Korver, O. and M.B. Katan, *The Elimination of Trans Fats from Spreads: How Science Helped to Turn an Industry Around*. Nutrition Review, 2006. **64**(6): p. 275–279.

[3] Brouwer, I.A., et al., *Effect of Animal and Industrial Trans Fatty Acids on HDL and LDL Cholesterol Levels in Humans--a Quantitative Review*. PLos One, 2010. **5**(3): p. 9434.

[4] Hunter, J.E., *Dietary Levels of Ttrans-fatty Acids: Basis for Health Concerns and Iindustry Efforts to Limit Use*. Nutrition Review, 2005. **25**: p. 499–513.

[5] Drewnowski, A., *Sensory Properties of Fats and Fat Replacements*. Nutrition Review, 1992. **50**(4): p. 17–20.

[6] Grigelmo-Miguel, N., et al., *Influence of the Addition of Peach Dietary Fiber in Composition, Physical Properties and Acceptability of Reduced-fat Muffins*. Food Science and Technology International, 2001. **7**(5): p. 425–431.

[7] Zoulias, E., et al., *Effect of Fat and Sugar Replacement on Cookie Properties*. Journal of the Science of Food and Agriculture, 2002. **82**(14): p. 1637–1644.

[8] Tarancón, P., et al., *Sunflower Oil–water–cellulose Ether Emulsions as Trans-fatty acid-free Fat Replacers in Biscuits: Texture and Acceptability Study*. Food Bioprocess Technology, 2012. **6**(9): p. 2389–2398.

[9] Willet, W.C. and A. Ascherio, *Trans Fatty Acids: Are the Effects only Marginal ?* American Journal of Public Health, 1994. **84**(5): p. 722–724.

[10] Mensink, R.P., *Estimated Intakes of Trans Fatty and Other Fatty Acids in the US Population*. Journal of the American Dietetic Association, 1999. **99**: p. 166–174.

[11] Labarthe, D.R., *Urinary Sodium Excretion and Cardiovascular Disease Mortality*. Journal of the American Medical Association, 2006. **306**(10): p. 1084–1085.

[12] Roe, M. and H. Pinchen, *Trans Fatty Acids in a Range of UK Processed Foods*. Food Chemistry, 2013. **140**: p. 427–431.

[13] Mensink, R.P., et al., *Effects of Dietary Fatty Acids and Carbohydrates on the Ratio of Serum Total to HDL Cholesterol and on Serum Lipids and Apolipoproteins: a Meta-analysis of 60 Controlled Trials*. American Journal Clinical Nutrition, 2003. **77**(5), p. 1146–1155.

[14] Menaa, F., et al., *Technological Approaches to Minimize Iindustrial Trans Fatty Acids in Foods*. Journal of Food Science, 2013. **78**(3): p. R377–386.

[15] Bendsen, N.T., et al., *Consumption of Iindustrial and Ruminant Trans Fatty Acids and Risk of Coronary Heart Disease: a Systematic Review and Meta-analysis of Cohort Studies*. European Journal of Clinical Nutrition, 2011. **65**(7): p. 773–783.

[16] Rogers, M.A., et al., *Engineering the Oil Binding Capacity and Crystallinity of Self-assembled Fibrillar Networks of 12-Hydroxystearic Acid in Edible Oils*. Soft Matter, 2008. **4**(6): p. 1147.

[17] Co, E.D. and A.G. Marangoni, *Organogels: an Alternative Edible Oil-structuring Method.* Journey of the American Oil Chemists Society, 2012. **89**(5): p. 749–780.

[18] Pernetti, M., et al., *Structuring of Edible Oils by Alternatives to Crystalline Fat*. Current Opinion in Colloid & Interface Science, 2007. **12**(4–5): p. 221–231.

[19] Murdan, S., et al., *Novel Gels and Their Dispersions--Oral Drug Delivery Systems for Ciclosporin.* International Journal of Pharmacertics, 2005. **300**(1–2): p. 113–124.

[20] Vintiloiu, A. and J.C. Leroux, *Organogels and Their Use in Drug Delivery--a Review*. Journal of Controlled Release, 2008. 125(3): p. 179–192.

[21] Jibry, N. and S. Murdan, *In Vivo Investigation, in Mice and in Man, into the Irritation Potential of Novel Amphiphilogels Being Studied as Transdermal Drug Carriers*. European Journal of Pharmaceutics and Biopharmaceutics, 2004. **58**(1): p. 107–119.

[22] Terech, P., et al., *Structures of Organogels Based upon Cholesteryl 4-(2-anthryloxy)butanoate, a Highly Efficient Luminescing Gelator: Neutron and X-ray Small-angle Scattering Investigations.* Journal of Physical Chemistry, 1995. 99(23): p. 9558–9566.

[23] Wu, S., et al., *Solvent-induced Polymorphic Nanoscale Transitions for 12-Hydroxyoctadecanoic Acid Molecular Gels*. Crystal Growth & Design, 2013. **13**: p. 1360–1366.

[24] Mallia, V.A., et al., *Robust Organogels from Nitrogen-containing Derivatives of (R)-12-hydroxystearic Acid as Gelators: Comparisons with Gels from Stearic Acid Derivatives*. Langmuir, 2009. **25**(15): p. 8615–8625.

[25] Marangoni, A.G., *Crystallography*, in *Fat Crystal Networks*, A.G. Marangoni, Editor. 2005, Marcel Dekker: New York. p. 1-20.

[26] Rogers, M.A., et al., *Nanostructuring Fiber Morphology and Solvent Inclusions in 12-Hydroxystearic Acid / Canola Oil Organogels.* Current Opinion in Colloid & Interface Science, 2009. **14**(1): p. 33–42.

[27] Maskaev, A.K., et al., *Preparation of 12-Hydroxystearic Acid, the Raw Material for Plastic Greases.* Chemistry and Technology of Fuels and Oils, 1971. **7**(2): p. 109–112.

[28] Graham, T., *Liquid Diffusion Applied to Analysis*. Philosophical Transaction of Royal Society of London, 1861. **151**: p. 183–224.

[29] Lloyd, D.J., *The Problem of Gel Structure*, in *Colloid Chemistry: Theoretical and Applied*, J. Alexander, Editor. 1926, The Chemical Catalog Co.: New York. p. 767-782.

[30] Hermans, P.H., *Gels*. Colloid Science, 1949. **II**: p. 483–651.

[31] Weiss, R.G. and P. Terech, *Introduction*, in *Molecular Gels: Materials with Self-Assebled Fibrillar Networks*, R.G. Weiss and P. Terech, Editors. 2006, Springer: Dordrecht, The Neatherlands. p. 1-13.

[32] Raghavan, S.R. and J. F. Douglas, *The Conundrum of Gel Formation by Molecular Nanofibers, Wormlike Micelles, and Filamentous Proteins: Gelation without Cross-links?* Soft Matter, 2012. **8**(33): p. 8539.

[33] Hirst, A.R., et al., *Low-molecular-weight Gelators: Elucidating the Principles of Gelation Based on Gelator Solubility and a Cooperative Self-assembly Model*. Journal of American Chemistry Society, 2008. **130**(28): p. 9113–9121.

[34] Gesser, H.D. and P.C. Goswami, *Aerogels and Related Porous Materials*. Chemical Reviews, 1989. **89**: p. 765–788.

[35] Rogers, M.A. and A.G. Marangoni, *Solvent-modulated Nucleation and Crystallization Kinetics of 12-Hydroxystearic Acid: a Nonisothermal Approach*. Langmuir, 2009. **25**(15): p. 8556–8566.

[36] Terech, P. and R.G. Weiss, *Low Molecular Mass Gelators of Organic Liquids and the Properties of Their Gels.* Chemical Reviews, 1997. **97**(8): p. 3133–3160.

[37] Lam, R., et al., *A Molecular Insight into the Nature of Crystallographic Mismatches in Self-assembled Fibrillar Networks under Non-isothermal Crystallization Conditions*. Soft Matter, 2009. **6**(2): p. 404.

[38] Li, J.L., et al., *Architecture of a Biocompatible Supramolecular Material by Supersaturation-driven Fabrication of Its Fiber Network.* Journal of Physical Chemistry, 2005. **109**(51): p. 24231–24235.

[39] Liu, X.Y., et al., *Creating New Superamolecular Materials by Architecture of Three-dimensional Nanocrystal Fiber Networks*. Journal of American Chemistry Society, 2002. 124: p. 15055-15063.

[40] Moffat, J.R. and D.K. Smith, *Controlled Self-sorting in the Assembly of 'Multi-gelator' Gels*. Chemical Communications, 2009. 3: p. 316–318.

[41] Chen, J., et al., *Analyte-triggered Gelation : Initiating Self-assembly via Oxidation-induced Planarization*. Journal of American Chemistry Society, 2008. **130**: p. 16496–16497.

[42] Sahoo, S., et al., *Organogels: Properties and Applications in Drug Delivery*. Designed Monomers and Polymers, 2011. **14**(2): p. 95–108.

[43] Abdallah, D.J. and R.G. Weiss, *N-alkanes Gel (and Many Other Organic Liquids)*. Langmuir, 2000. **16**(10): p. 352–355.

[44] Li, J.L. and X.Y. Liu, *Soft Fibrillar Materials: Fabrication and Applications*. 2013. Wiley-VCH: Germany.

[45] Wang, R., et al., *Architecture of Fiber Network: from Understanding to Engineering of Molecular Gels.* Journal of Physical Chemistry, 2006. **110**: p. 25797–25802.

[46] Wang, R., et al., *Real-Time Observation of Fiber Network Formation in Molecular Organogel : Supersaturation-dependent Microstructure and Its Related Rheological Property*. Journal of Physical Chemistry, 2006. **110**: p. 7275–7280.

[47] Liu, X.Y., *From Solid-fluid Interfacial Structure to Nucleation Kinetics: Principles and Strategies for Micro/nanostructure Engineering*, in *Nanoscale Structure and Assembly at Solid-Fluid Interfaces*, X.Y. Liu and J.J. De Yoreo, Editors. 2004, Kluwer Acdemic: New York.

[48] Li, J.L., et al., *Engineering of Small Molecule Organogels by Design of the Nanometer Structure of Fiber Networks*. Advanced Materials, 2006. **18**(19): p. 2574–2578.

[49] Rogers, M.A. and A.G. Marangoni, *Solvent-modulate Nucleation and Crystallization Kinetics of 12-Hydroxystearic Acid: a Nonisothermal Approach.* Langmuir, 2009. **25**(15): p. 8556–8566.

[50] Hamer, M.A., et al., *Organogel Particles*. U.S. Patent 6,858,666, Feb 22, 2005.

[51] Liu, G., et al., *Rheological Studies of Alkylamine-ethylene Glycol Organogel: Chain Length Dependent Structural Diversity*. Colloids and Surfaces A-Physicochemical and Engineering Aspects, 2013. **434**: p. 1–8.

[52] Elliger, C.A., et al., *Thickening Action of Hydroxystearates in Peanut Butter.* Journal of the American Oil Chemists Society, 1972. **49**: p. 536–537.

[53] Pénzes, T., et al., *Rheological Analysis of the Structural Properties Effecting the Percutaneous Absorption and Stability in Pharmaceutical Organogels*. Rheologica Acta, 2004. **43**(5): p. 457–463.

[54] Pénzes, T., et al., *Topical Absorption of Piroxicam from Organogels—In Vitro and In Vivo Correlations*. International Journal of Pharmaceutics, 2005. **298**(1): p. 47–54.

[55] Kuwahara, T., et al., *Crystal Structure of DL-12-hydroxystearic Acid*. Chemistry Letters, 1996. **25**(6): p. 435–436.

[56] Terech, P., et al., *Organogels and Aerogels of Racemic and Chiral 12-Hydroxyoctadecanoic Acid*. Langmuir, 1994. **10**(10): p. 3406–3418.

[57] Eloundou, J.P., et al., *Calorimetric and Rheological Studies of 12-Hydroxystearic Acid / Digycidyl Ether of Bisphenol a Blends*. Polymer Bulletin, 2005. **53**(5–6): p. 367–375.

[58] Humphrey, K.L. and S.S. Narine, *Lipid Phase Behavior*, in *Fat Crystal Networks*, A.G. Marangoni, Editor. 2005, Marcel Dekker: New York. p. 83–114.

[59] Rogers, M.A., et al., *Post-crystallization Increases in the Mechanical Strength of Self-assembled Fibrillar Networks is due to an Increase in Network Supramolecular Ordering*. Journal of Physics D-Applied Physics, 2008. **41**(21): p. 215501.

[60] Raynal, M. and L. Bouteiller, *Organogel Formation Rationalized by Hansen Solubility Parameters.* Chemical Communications, 2011. **47**(29): p. 8271–8273.

[61] Gao, J., et al., *Harnessing Hansen Solubility Parameters to Predict Organogel Formation.* Journal of Materials Chemitry, 2012. **2**(2): p. 1–8.

[62] Hanabusa, K., et al., *Low Molecular Weight Gelators for Organic Fluids: Gelation Using a Family of Cyclo(dipeptide)s*. Journal of Colloid and Interface Science, 2000. **224**(2): p. 231–244.

[63] Hirst, A.R. and D.K. Smith, *Solvent Effects on Supramolecular Gel-phase Materials: Ttwo-component Dendritic Gel*. Langmuir, 2004. **20**(25): p. 10851–10857.

[64] Hansen, C.M., *Solubility Parameters : an Introduction*, in *Hansen Solubility Parameters: A User's Handbook*. 1999, CRC Press: Boca Raton, FL. p. 1–23.

[65] Hildebrand, J.H., *Factors Determining Solubility among Non-electrolytes*. Proceedings of the National Academy of Sciences, 1950. **36**(1): p. 7–15.

[66] Hildebrand, J.H. and R.L. Scott, *The Solubility of Nonelectrolytes*. 1959, Dover Publications: Reinhold, NY.

[67] Wang, S., et al., *Hansen Solubility Parameter Analysis on the Dispersion of Zirconia Nanocrystals.* Journal of Colloid and Interface Science, 2013. **407**(0): p. 140–147.

[68] Hansen, C.M. and K. Skaarup, *The Three Dimensional Solubility Parameter - Key to Paint Component Affinities III. - Independent Calculation of the Parameter Components.* Journal of Paint Technology, 1967. **39**(511): p. 511–514.

[69] Redelius, P., *Hansen Solubility Parameters of Asphalt, Bitumen, and Crude Oils*, in *Hansen Solubility Parameters: A User's Handbook*. 1999, CRC Press: Boca Raton, FL. p. 159.

[70] Marangoni, A.G. and S.S. Narine, *Rheology Fundamentals and Structural Theory of Elasticity*, in *Fat Crystal Networks*, A.G. Marangoni, Editor. 2005, Marcel Dekker: New York. p. 115–142.

[71] Duffy, P., *XVIII.—On Certain Isomeric Transformations of Fats*. Quarterly Journal of Chemical Society, 1853. **5**: p. 197–210.

[72] Clarkson, C.E. and T. Malkin, *An X-ray and Thermal Examination of the Glycerides; the Polymorphism of Simple Triglycerides.* Journal of American Chemistry Society, 1948. **1**, p. 985–987.

[73] Campos, R., *Experimental Methodology*, in *Fat Crystal Networks*, A.G. Marangoni, Editor. 2005, Marcel Dekker: New York. p. 267–348.

[74] Timms, R.E., *Phase Behaviour of Fats and Their Mixtures*. Progress in Lipid Research, 1984. **23**(1): p. 1–38.

[75] Hagemann, J.W. and J.A. Rothfus, *Effects of Chain Length, Conformation and α-Form Packing Arrangement on Theoretical Monoacid Triglyceride ß-Forms.* Journal of the American Oil Chemists' Society, 1988. **65**(4): p. 638–646.

[76] Larsson, K., *Liquid-crystalline Lipid-water Phases*, in *Lipids: molecular organization, physical functions and technical applications*, K. Larsson, Editor. 1994, The Oily Press: Dundee, Scotland. p. 47.

[77] deMan, J.M., *X-ray Diffraction Spectroscopy in the Study of Fat Polymorphism*. Food Research International, 1992. **25**(6): p. 471–476.

[78] Rhodes, G., *Collecting Diffraction Data*, in *Crystallography Made Crystal Clear: A Guide for Users of Macromolecular Models*, J. Hayhurst, Editor. 2006, Academic Press: UK. p. 49–90.

[79] Watson, E.S., et al., *A Differential Scanning Calorimeter for Quantitative Differential Thermal Analysis.* Analytical Chemistry, 1964. **36**(7): p. 1233–1238.

[80] F. Shahidi and P. K. J. P. D. Wanasundara, "Extraction and analysis of lipids," in *Food Lipids: Chemistry, Nutrition, and Biotechnology*, C. C. Akoh and D. B. Min, Ed., 2nd ed. New York: Marcel Dekker, 2002, pp. 159–161.

[81] Farrar, T.C., *An Introduction To Pulse NMR Spectroscopy*. 1987, Farragut Press: Knoxville, TN.

[82] Sakurai, T., et al., *A Comparative Study on Chiral and Racemic 12-Hydroxyoctadecanoic Acids in the Solutions and Aggregation States: Does the Racemic form Really Form a Gel*? Bulletin of the Chemical Society of Japan, 2010. **83**(2), p. 145–150.

[83] Settle, F.A., *Infrared Spectroscopy*, in *Handbook of Instrumental Techniques for Analytical Chemistry*. 1997, Prentice Hall: Upper Saddle River, NJ. p. 247–284.

3.0 Solvent Induced Polymorphic Nanoscale Transitions for 12-Hydroxystearic Acid Molecular Gels

Wu, S.,[1] Gao, J.,[1] Emge, T.J.,[2] and Rogers, M.A.[1]*

1) School of Environmental and Biological Sciences, Department of Food Science, Rutgers University; The State University of New Jersey, New Brunswick, NJ 08901

2) School of Arts and Science, Department of Chemistry and Chemical Biology, Rutgers University; The State University of New Jersey; Piscataway, NJ 08854

**This chapter is published in *Crystal Growth & Design* (DOI 10.1021/cg400124e), Received: January 22, 2013 / Published: February 5, 2013.

*Corresponding Author: Michael A. Rogers, Department of Food Science; Rutgers University; The State University of New Jersey, New Brunswick, NJ.
rogers@AESOP.Rutgers.edu

3.1 Abstract

12-hydroxystearic acid (12HSA) molecular gels have been reported to form self-assembled fibrillar network (SAFiNs) in organic solvents. For the first time, different polymorphic forms for 12HSA molecular gels have been reported. 12HSA, in alkanes and thiols, have a hexagonal sub cell spacing (~4.1 Å) and are arranged in a multi-lamellar fashion with a distance greater than the bi-molecular length of 12HSA (~54 Å). This polymorphic form corresponded to SAFiN with CGC less than 1 wt%. 12HSA, in nitriles, aldehydes and ketones, have a triclinic parallel sub cell (~ 4.6, 3.9, and 3.8 Å) and interdigitation of the lamellar structure (38 to 44 Å). This polymorphic form corresponds to a less effective sphereultic supramolecular crystalline network, which immobilizes solvents at CGC greater than 1.5 wt%.

3.2 Introduction

Molecular organogels are thermally reversible, quasi-solid materials comprised of an organic liquid (usually ≥ 95 %) and a gelator molecule that self-assemble via physical interactions, including hydrogen-bonding,[1-4] π-π stacking,[5] dipole-dipole,[6, 7] and London dispersion forces,[8] into a 3-dimensional network.[9-11] Although the physical interactions between gelator molecules are central in understanding gelation, the solvent-gelator specific (i.e., H-bonding) and nonspecific (dipole-dipole, dipole-induced and instantaneous dipole induced forces) intermolecular interactions are equally important.[12, 13] The process of self-assembly, in molecular gels, is an intricate process that must balance the solubility and those intermolecular forces that control epitaxial growth into axially symmetric elongated aggregates.[10, 13-16] During assembly, individual molecules are driven to assemble by molecular self-recognition and intermolecular non-covalent interactions into oligomers and subsequently, these oligomers assemble into fibrillar aggregates immobilizing the solvent via capillary forces.[17, 18]

Herein, we present an investigation of the first polymorphic transformation, for a molecular gel, induced by modifying the solvent with 12HSA as the gelator. In molecular gels, polymorphic transitions have only been noted in (R)-18-(n-alkylamino)octadecan-7-ols in CCL_4 which undergoes a gel-gel polymorphic transition during heating.[9] Several other transitions have been reported in molecular gels however differences lie at the supramolecular level of structure induced by crystallographic mismatches and not different polymorphic forms.[2, 3, 12, 15, 19-22]

12HSA, a structurally simple, highly effective low molecular weight gelator (LMOG), has been studied extensively for gelation kinetics[2, 23-25] and supramolecular structure formation,[3, 19, 20, 26-28] as well as to monitor surface properties,[29] solvent polarity,[15, 30] the influence of minor components,[31] and effects of chemical structure.[30, 32-36] Zhu and Dordick have eloquently articulated that the heterogeneous nature of organogels consists of critical interactions between the solvent and gelator, and it is those interactions that govern the physical behavior and gelation process.[12] Molecular assembly begins, in LMOGs, once a critical concentration is reached, below which the gelator is soluble and exists as monomers in solution.[12] Once the critical concentration is reached, the gelation process begins leading to a decrease of gelator in the solution phase.[12] Further addition of gelator molecules causes the solvent to be immobilized but does not effect the soluble concentration of the gelator.[12] Since gelator solubility is strongly dependent on the nature of the solvent, most studies stop at correlating critical gelator concentration (CGC) to solubility parameters. [12, 13] Typically, studies that examine the effect of solvent often focus on solubility parameters because excellent correlations between solubility and CGC exist and nuisances in molecular assembly affecting the CGC remain relatively unknown. In this current work, we examine 12HSA in several solvents to study the nanostructure and microstructure of the molecular gels.

3.3 Method

Solvent selection criteria were maintained as simply as possible with the aliphatic chain being linear, saturated, the functional group located in the primary position and the solvent must be in a liquid state between 10 and 30 ^{o}C. The only exceptions to these

selection criteria were the ketones where the functional group was located in the exact middle of the molecule. Apolar solvents included the aliphatics, polar solvents were subdivided into three categories: aldehydes, ketones, and nitriles; as well, the solvents capable of hydrogen bonding and forming a molecular gel were only the thiols. A complete list of the employed solvents and their solubility parameters may be found in Gao et al.[13] All solvents and R-12-hydroxystearic acid (12HSA) were obtained from Sigma-Aldrich (Cherry Hill, NJ, USA) with purity greater than 0.95%.

The supramolecular structure was imaged using a Linkham imaging station (Linkham, Surrey, England) equipped with a Q imagining 2560 x 1920 pixel CCD camera (Micropublisher, Surrey, Canada) and a 10 X Olympus lens (0.25 N.A.) (Olympus, Tokyo, Japan). Samples were placed on a glass slide with a cover slip on top of the sample. The slide was transferred into a peltier temperature control stage (LTS120, Linkham, Surrey, England) and heated to 80 ^{o}C and was slowly cooled (2 ^{o}C/min to 20 ^{o}C) to observe supramolecular network formation.

The x-ray diffraction (XRD) or wide-angle x-ray scattering (WAXS) patterns of several samples containing 12HSA gel in different solvents were obtained by use of a Bruker HiStar area detector and an Enraf-Nonius FR571 rotating anode x-ray generator equipped with Rigaku Osmic mirror optic system (~0.06 deg 2q nominal dispersion for Cu Ka; l = 1.5418 Å) operating at 40 kV and 40 mA. All of the data were collected at room temperature over a period of about 300 sec. The sample to detector distance was 10.0 cm and the standard spatial calibration was performed at that distance. Scans were 4 degrees wide in omega (w) with fixed detector, or Bragg, angle (2q) of 0 deg, and fixed

platform (*f* and *c*) angles of 0 and 45 deg, respectively. In all cases, the count rate for the area detector did not exceed 100,000 cps.

The carbonyl (~1700 cm^{-1}) and hydroxyl (~3200 cm^{-1}) signals were measured using a Thermo Nicolet FT-IR and an Attenuated total refraction (ATR) prism (Thermo Fisher Scientific, MA, USA). 256 scans were collected at a resolution of 4 cm^{-1}.

3.4 Discussion

Recent work found the CGC of 12HSA is strongly influenced by solvent parameters varying between 0.2 wt% to nearly 3.0 wt% (Table 1).[13] Solvent parameters influence the supramolecular structure of gelators, where the interaction between the solvent and gelator induce changes in the thickness, the number of junction zones and the sense of helical twist.[12, 18] For symmetrical trehalose diesters, a class of super gelators, the gelation number varies between 12000 and 100 depending on the solvent.[12] In this work, Zhu and Dordick illustrate that the fiber thickness and morphology influences the gelation number, which correlates to the CGC. [12] In the solvents selected for this study with 12HSA as the molecular gelator, not only did the CGC vary but also the melting temperature of the molecular gels from 65 ^{o}C to 32 ^{o}C (Table 1). The melting temperatures were determined from the peak of the differential scanning calorimetry thermograms (Supplemental Figures 3-1~3-3). Melting temperatures could not be obtained for all samples because several solvents were too volatile. Previously, it has been established that the melting temperature of the molecular gel is dependent on the supramolecular structure of the fibers, where thinner fibers melt at lower temperatures than thicker fibers, in other words, as the crystalline perfection

increases so does the melting point.[28, 30] However, these changes in melting points are relatively minor compared to the changes we observed in this study.

Table 1: Critical gelator concentrations from reference [13] and peak melting temperatures determined in triplicate using differential scanning calorimetry.

Solvent	CGC (wt%)	Melting Temperature (^{o}C)
Hexane	**0.4**	**61.9±0.01**
Heptane	**0.3**	**62.5±0.1**
Octane	**0.3**	**61.6±0.5**
Nonane	**0.25**	**60.5±0.9**
Decane	**0.2**	**63.9±0.1**
Tetradecane	**0.2**	**64.8±0.35**
1-Pentanethiol	**0.5**	**NA**
1-Hexanethiol	**0.45**	**45.7±0.01**
1-Heptanethiol	**0.45**	**49.1±0.03**
1-Octanethiol	**0.4**	**50.8±0.04**
1-Decanethiol	**0.3**	**51.9±0.06**
Butylnitrile	**2.1**	**64.2±0.3**
Hexanenitrile	**1.9**	**65.5±1.2**
Heptylnitrile	**1.5**	**58.4±1.0**
Nonanenitrile	**0.9**	**NA**
Butylaldehyde	**2.8**	**NA**
dodecylaldehyde	**1.4**	**41.2±0.57**
4-Heptone	**2**	**NA**
5-nonanone	**2.1**	**32.8±0.8**
6-undecanone	**1.6**	**45.6±1.5**

On a supramolecular level, the fibrillar structure of 12HSA molecular gels varies depending on the solvent (Figure 3-1~3-3). For 12HSA molecular gels in alkanes (Figure 3-1 A, B) the aspect ratio of the nanofibers is very large. The large aspect ratio and thin fiber morphology results in a high surface area and which in turn allows for very low CGC and high gelation numbers. As the alkane chain length increases, the CGC

decreases and the fibers length increases (Figure 3-1). In select thiols, capable of forming weak hydrogen bonds, the cohesive energy density increases (varying between 17 to 18 $MPa^{1/2}$) compared to alkanes (varying between 15 and 16 $MPa^{1/2}$) due to the weak hydrogen bonding and polar component.[13, 37] The supramolecular structure is affected by the change in solubility parameters to produce shorter fibers, which are thinner than in the alkanes (Figure 3-2 A, B). Although there is a drastic change in the supramolecular structure, the overall fiber morphology is still very effective at entraining the solvent forming a molecular gel at low CGCs (Table 1). In polar solvents (nitriles (Figure 3-3 A, B); aldehydes (Figure 3-3 C, D); ketones (Figure 3-3 E, F) the supramolecular structure varies greatly compared to the alkanes and nitriles. The cohesive energy density is higher in nitriles (17 to 25 $MPa^{1/2}$), aldehydes (17 to 18 $MPa^{1/2}$), and ketones (18 to 20 $MPa^{1/2}$) compared to the alkanes and thiols. The supramolecular structure varies significantly in the different classes of polar solvents (Figure 3-3). Although all of the solvents still form molecular gels, the CGC is considerably higher, ranging between 0.9 and 2.8 wt% and the opacity of the gels increases. The supramolecular structure also changes from high aspect ratio fibers to spherultic-like aggregates. In acetonitrile (Figure 3-3 A) radial growth from central nuclei occurs until adjacent crystals impede their growth. As the chain length of the nitriles increases, the supramolecular crystal structure varies become thinner lowering the CGC (Figure 3-3 B). 12HSA molecular gels in aldehydes (Figure 3-3 C, D) and ketones (Figure 3-3 E, F) have the highest CGC and opacity.[13] The supramolecular crystalline structure does not effectively entrain the solvent due to the colloidal crystal structure. Although there are some fiber-like structures the supramolecular network does not

resemble what is observed in neither alkanes (Figure 3-1) nor thiols (Figure 3-2). At first, it was assumed that the solvent parameters varied the supramolecular structures, however, this did not explain the differences in the melting temperatures. This compelled us to examine the possibility that there may be differences at the nano level of structure; meaning different polymorphic forms may exist within molecular gels of 12HSA.

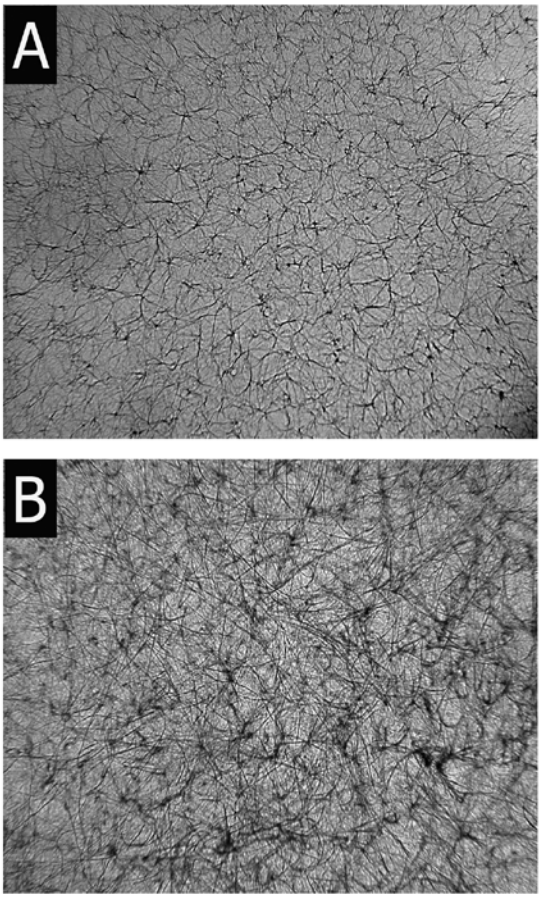

Figure 3-1: Brightfield microscope images of molecular gels of 2 wt% 12-hydroxystearic acid in hexane (A) and dodecane (B). Width of micrograph is 120 μm.

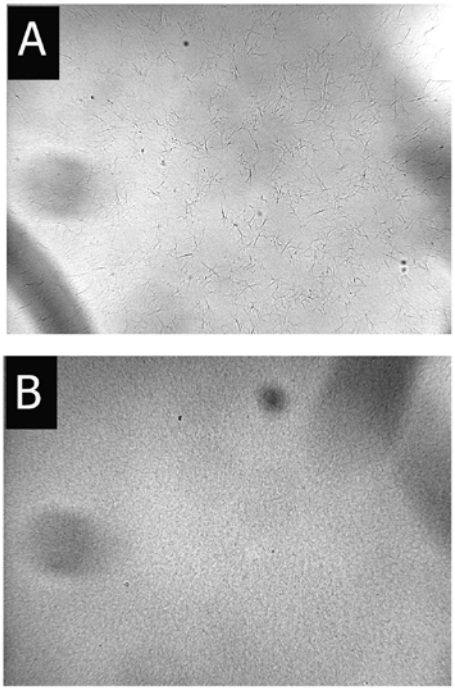

Figure 3-2: Brightfield microscope images of molecular gels of 2 wt% 12-hydroxystearic acid in pentanethiol (A) and decanethiol (B). Width of micrograph is 120 μm.

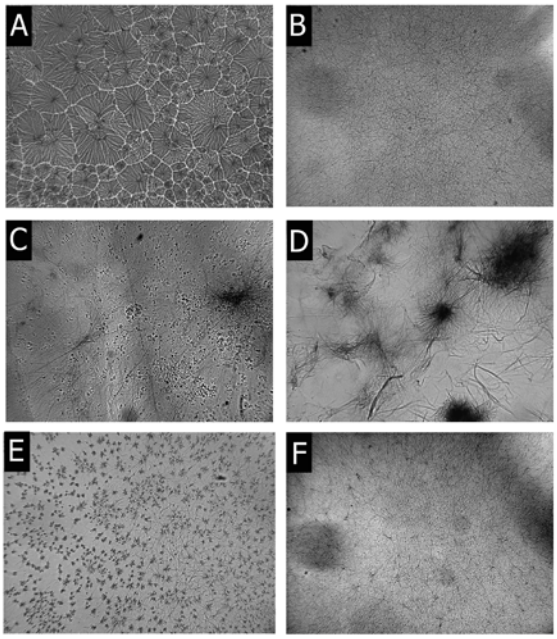

Figure 3-3: Brightfield microscope images of molecular gels of 2 wt% 12-hydroxystearic acid in acetonitrile (A) and octanenitrile (B), butylaldehyde (C), decanal (D), heptone (E), and undecanone (F). Width of micrograph is 120 μm.

With drastic differences in the microstructure, the nanostructure was probed to study if there was a correlation with the crystal morphology. X-ray diffraction (XRD) was used to measure the wide- and short-angle spacings of the molecular gels. The X-ray diffractograms for all alkanes had very similar diffraction patterns with a short-angle spacing of 53.5 Å and a hlk higher order reflection at 15.2 Å (Figure 3-4 A). The presence of the higher order reflection indicates a muti-lamellar crystal configuration. The lamellar thickness of 12HSA should correlate to approximately twice the extended molecular length of 12HSA (~46 Å).[30] In alkanes it appears that a swollen lamellar network is present which has been previously reported.[26] The wide-angle spacing at 4.3 Å corresponds to hexagonal (~4.1 Å) sub-cell spacings (Figure 3-4 B).[38, 39] Observing the FT-IR spectrogram, the peak corresponding to the carboxyl acid dimerization at 1690 cm^{-1} was observed which is typical for hydroxystearic acid molecular gels (Figure 3-5 A).[2, 40, 41] The peak corresponding to the hydroxyl hydrogen bonding, appearing as a broad peak at 3200 cm^{-1} indicates that the hydroxyl groups at position 12 are involved in hydrogen bonds (Figure 3-5 B).

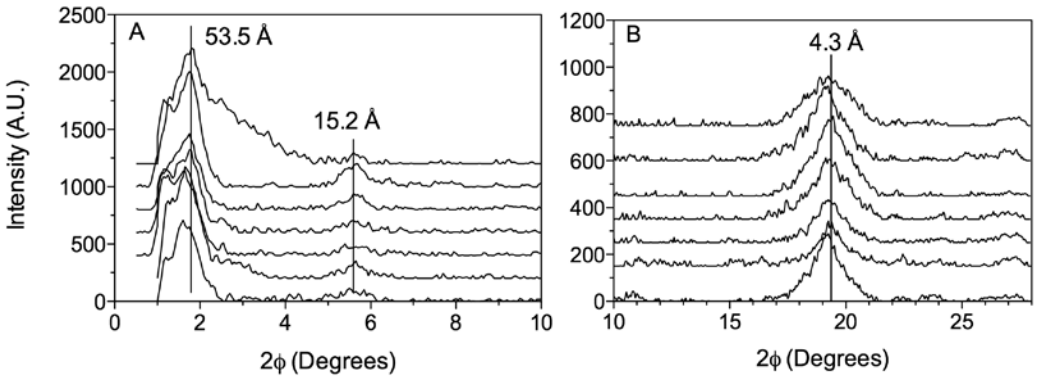

Figure 3-4: Vertically offset wide-angle (A) and short-angle sub cell spacings (B) for 2 wt% 12HSA in aliphatic solvents. The diffractrograms from bottom to the top are hexane, heptane, octane, nonane, decane, dodecane, tetradecane.

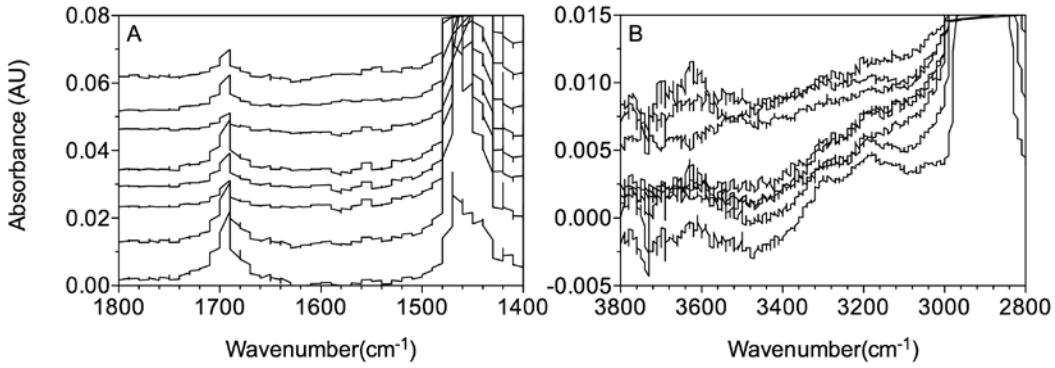

Figure 3-5: Vertically offset FT-IR spectra focusing on the carboxylic acid region (A) and hydroxyl region (B), using the air as the background. The diffractrograms from bottom to the top are hexane, heptane, octane, nonane, decane, dodecane, tetradecane.

Although the network structure was finer in molecular gels containing thiols than was observed in alkanes, the entrainment of the solvent by the fibrillar network was similar (Figure 3-1 and 3-2). In selected thiols, similar short-angle spacings (Figure 3-6 A) and wide-angle spacings (Figure 3-6 B) are observed indicating a hexagonal spacing with a multi-lamellar crystal lattice equal to an extended bi-molecular length. The FT-IR spectrograms indicate a cyclic dimmer between the carboxylic acid head groups (Figure 3-7 A) and the broad weak peak at 3200 cm-^{1} indicates that there is an absence of free hydroxyl groups (Figure 3-7 B).

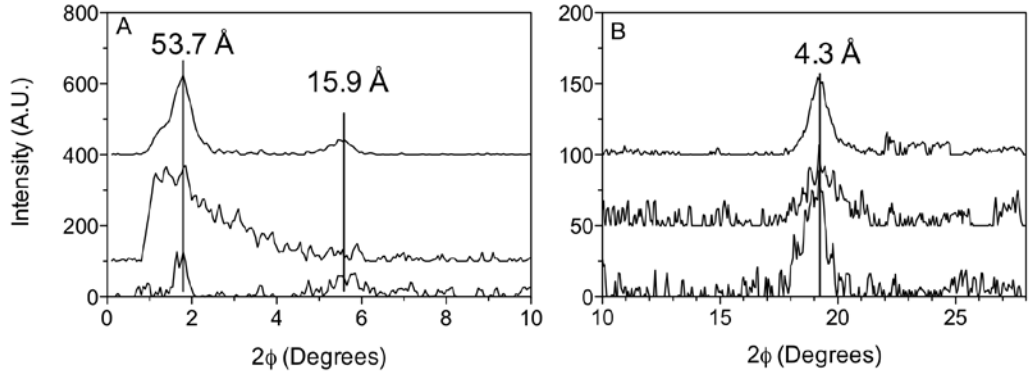

Figure 3-6: Vertically offset wide-angle (A) and short-angle sub cell spacings (B) for 2 wt% 12HSA in thiol based solvents. The diffractograms from bottom to the top are hexanethiol, hexanethiol, and decanethiol.

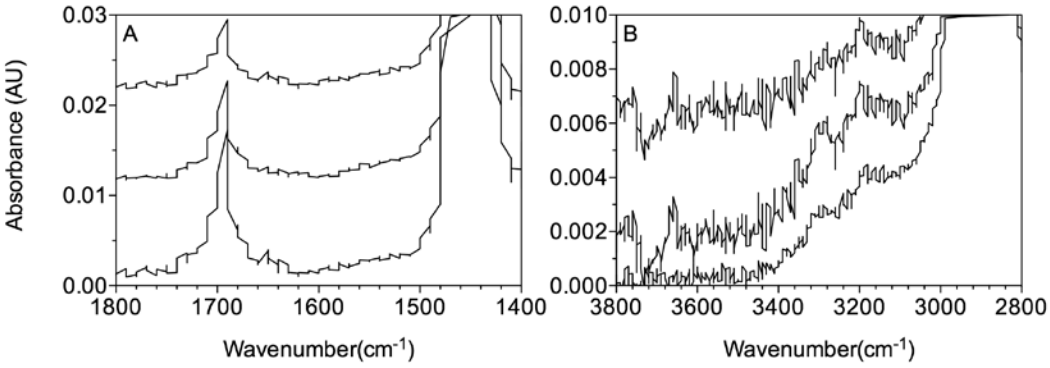

Figure 3-7: Vertically offset FT-IR spectra focusing on the carboxylic acid region (A) and hydroxyl region (B), using the air as the background. The diffractograms from bottom to the top are hexanethiol, hexanethiol, and decanethiol.

In polar solvents, including nitriles, aldehydes and ketones (Figure 3-3) the CGC (CGC> 1.5 wt%) drastically increased compared to the thiols and alkanes (CGC <1.0 wt%) (Table 1). This corresponds to changes in the supramolecular structures observed in the aforementioned solvents (Figure 3-1~3-3). In polar solvents (which have higher cohesive energy densities) the fibrillar crystal morphology is replaced with a spherultic-

like structure that is less effective at entraining solvents. On a nanoscale level, considerable changes in the molecular arrangement occurred. The short-angle spacings indicate a decrease of the lamellar spacing from ~53 Å to 44 Å for nitriles (Figure 3-8 A) and ketones (Figure 3-8 E) and ~39 Å for aldehydes (Figure 3-8 C). These changes are also reflected in the hlk higher order reflections. This reduction in the lamellar spacing is near the minimum of the bimolecular length for 12HSA (~46 Å) in nitriles and ketones and is significantly shorter for the aldehydes suggesting that there is an interdigitation of 12HSA in the multi-lamellar structures. With the change in the short-angle spacing, a polymorphic transition is also observed in the sub cell spacing. The hexagonal sub cell spacing observed in the fibrillar aggregates (~4.1 Å) gives way to a triclinic parallel sub cell (strong peak at 4.6 Å, and two weak peaks at 3.9 Å and 3.8 Å) in nitriles, aldehydes and ketones (Figure 3-8 A, C, D). In the aldehydes, only the 4.6 and 3.8 Å peak is visible but the presence of the peak at 3.8 Å indicates that it is unlikely to be in the hexagonal polymorphic form.

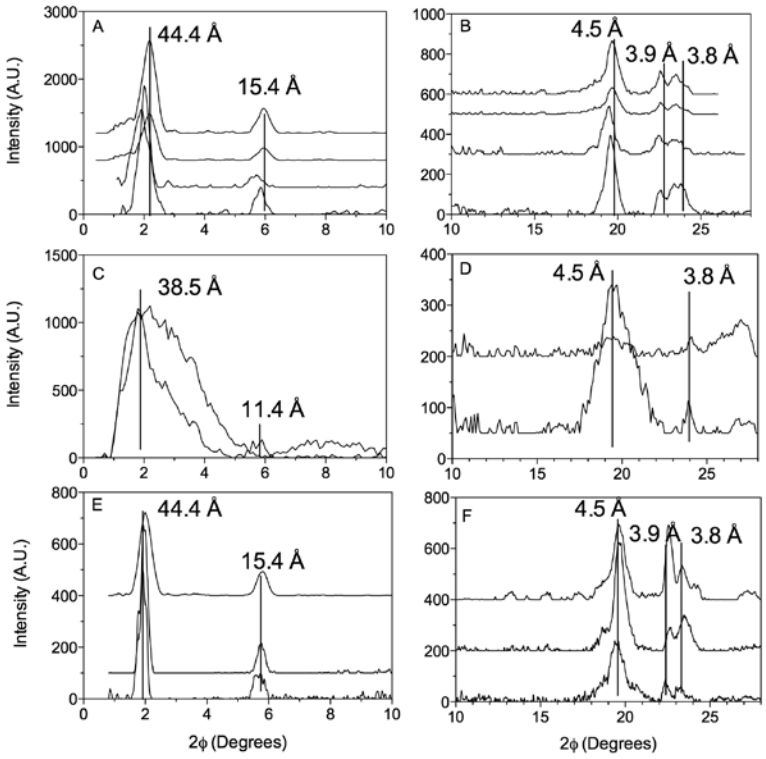

Figure 3-8: Vertically offset wide-angle (A,C,E) and short-angle sub cell spacings (B,D,F) for 2 wt% 12HSA in polar solvents. The diffractrograms from bottom to the top are (A,B) butylnitrile, hexanenitrile, heptylnitrile and nonanenitrile; (C,D) butylaldehyde and dodecylaldehyde;(E,F) heptone, nonanone and undecone.

Although the wide and short-angle spacings are similar for nitriles, aldehydes and ketones there are differences in relation to the non-covalent interactions between the 12HSA molecules (Figure 3-9). FT-IR shows that 12HSA in nitriles forms carboxylic acid dimmers (1690 cm^{-1}) (Figure 3-9 A). A broad peak is observed at 3600 cm^{-1} (Figure 3-9 B) indicating that hydroxyl groups, at position 12, form hydrogen bonds. Unlike the nitriles, the carboxylic acid groups in aldehydes (Figure 3-9 C) and ketones (Figure 3-9 E) do not form cyclic dimers (~1720 cm^{-1}). This in part would explain the reason why 12HSA molecule gels in aldehydes and ketones melt at temperatures much less than the other three sets of selected solvents. As well, the broad peak between 3200 and 3600 cm^{-}

[1] has the diffuse pattern suggesting that at least some of the hydroxyl groups are involved in hydrogen bonds. However, a new small peak is superimposed on the broad peak indicating there is substantial free hydroxyl groups in the molecular gels with aldehydes and ketones used as solvents. For the first time, two polymorphic forms (i.e., a hexagonal and triclinic parallel) are present in molecular gels (Figure 3-10), which result in changes at the microscopic and macroscopic levels of structure.

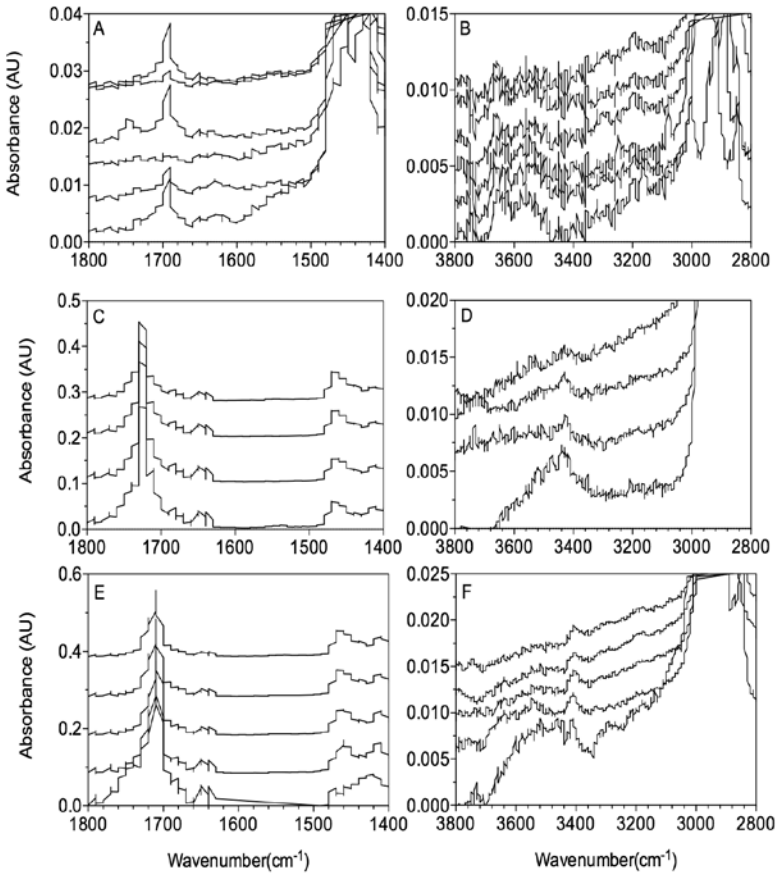

Figure 3-9: Vertically offset FT-IR spectra focusing on the carboxylic acid region (A) and hydroxyl region (B), using the air as the background. The diffractrograms from bottom to the top are (A,B) butylnitrile, hexanenitrile, heptylnitrile and nonanenitrile; (C,D) butylaldehyde and dodecylaldehyde;(E,F) heptone, nonanone and undecone.

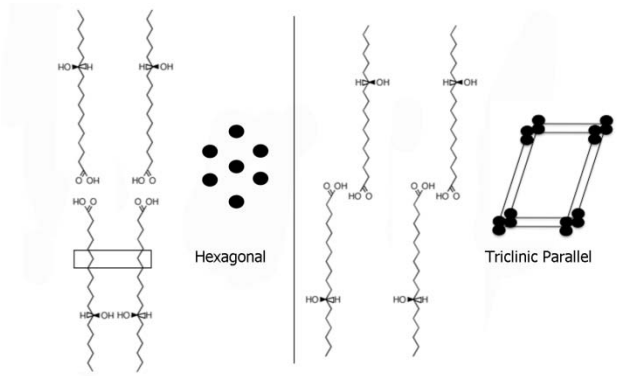

Figure 3-10: Schematic diagram of two polymorphic forms (hexagonal and triclinic parallel) of 12HSA in various solvents capable of forming molecular gels. The box represents the side view of the sub cell that is pictured next to the molecular structures.

3.5 Conclusion

12HSA is one of the most studied molecular gelators, in part due to its molecular simplicity, inexpensive cost and versatility in gelling numerous solvents. With so many studies on 12HSA in molecular gels it is amazing that no studies on polymorphism have been reported. In alkanes and thiols, a hexagonal sub cell spacing (~4.1 Å) and a multi-lamellar crystal morphology with a distance between lamella greater than the bi-molecular length of 12HSA. This polymorphic form corresponded to molecular gels with CGC less than 1 wt% and a supramolecular self assembled fibrillar network. 12HSA molecular gels in nitriles, aldehydes and ketones have a triclinic parallel sub cell (~ 4.6, 3.9, and 3.8 Å) and interdigitation in the lamellar. This polymorphic form is far less effective at immobilizing solvents with CGC greater than 1.5 wt% and a sphereultic supramolecular crystalline network.

3.6 Works Cited

1. Kuwahara, T., et al., *Crystal Structure of DL-12-Hydroxystearic Acid.* Chemistry Letters, 1996. **25**: p. 435-436.

2. Lam, R., et al., *A Molecular Insight into the Nature of Crystallographic Mismatches in Self-assembled Fibrillar Networks under Non-isothermal Crystallization Conditions.* Soft Matter, 2010. **6**(2): p. 404-408.

3. Li, J.L., et al., *Arichitecture of a Biocompatible Supramolecular Material by Supersaturation-Driven Fabrication of its Network.* Journal of Physical Chemistry B, 2005. **109**: p. 24231-24235.

4. Rogers, M.A., et al., *Multicomponent Hollow Tubules Formeed Using Phytosterol and γ-Oryzanol-Based Compounds: An Understanding of Their Molecular Embrace.* Journal of Physical Chemistry, 2010. **114**: p. 8278-8295.

5. Moffat, J.R. and D.K. Smith, *Controlled Self-Sorting in the Assembly of 'Multi-Gelator' Gels.* Chemical Communication, 2009. **3**: p. 316-318.

6. Brotin, T., J.P. Devergne, and F. Fages, *Photostationary Fluorescence Emission and Time Resoved Spectroscopy of Symmetrically Disubstituted Anthracenes on teh meso and Side Rings: The Unusual Behavior of the 1,4 Derivative.* Photochemistry and Photobiology, 1992. **55**: p. 349-358.

7. Terech, P., I. Furman, and R.G. Weiss, *Structures of Organogels Based Upon Cholesteryl 4-(2-Anthryloxy)Butanoate, A Highly Efficient Luminescing Gelator - Neutron AND X-Ray Small-Angle Scattering Investigations.* Journal of Physical Chemistry, 1995. **99**(23): p. 9558-9566.

8. Toro-Vazquez, J.F., et al., *Relationship Between Molecular Structure and Thermo-mechanical Properties of Candelilla Wax and Amides Derived from (R)-12-Hydroxystearic Acid as Gelators of Safflower Oil.* Food Biophysics, 2010. **5**(3): p. 193-202.

9. Mallia, V.A., et al., *Reversible Phase Transitions within Self-Assembled Fibrillar Networks of (R)-18-(n-Alkylamino)octadecan-7-ols in Their Carbon Tetrachloride Gels.* Journal of the American Chemical Society, 2011. **133**: p. 15045-15054.

10. Weiss, R.G. and P. Terech, *Introduction*, in *Molecular Gels: Materials with Self-Assebled Fibrillar Networks*, R.G. Weiss and P. Terech, Editors. 2006, Springer: Dordrecht, The Neatherlands. p. 1-13.

11. George, M. and R.G. Weiss, *Molecular Organogels. Soft Matter Comprised of Low-Molecular-Mass Organic Gelators and Organic Liquids.* Accounts of Chemical Research, 2006. **39**: p. 489-497.

12. Zhu, G. and J.S. Dordick, *Solvent Effect on Organogel Formation by Low Molecular Weight Molecules.* 2006. **18**(Chemistry of Materials): p. 5988-5995.

13. Gao, J., S. Wu, and M.A. Rogers, *Harnessing Hansen Solubility Parameters to Predict Organogel Formation.* Journal of Materials Chemistry, 2012. **22**: p. 12651-12658.

14. Suzuki, M., et al., *Effects of Hydrogen Bonding and van der Waals Interactions on Organogelation Using Designed Low-molecular-weight Gelators and Gel Formation at Room Temperature.* Langmuir, 2003. **19**(21): p. 8622-8624.

15. Rogers, M.A. and A.G. Marangoni, *Solvent-Modulated Nucleation and Crystallization Kinetics of 12-Hydroxystearic Acid: A Nonisothermal Approach.* Langmuir, 2009. **25**(15): p. 8556-8566.

16. Raynal, M. and L. Bouteiller, *Organogel Formation Rationalized by Hansen Solubility Parameters.* Chemical Communication, 2011. **47**: p. 8271-8273.

17. Hardy, J.G., A.R. Hirst, and D.K. Smith, *Exploring Molecular Recognition Pathways in One- and Two-component Gels Formed by Dendritic Lysine-based Gelators.* Soft Matter, 2012. **8**: p. 3399-3406.

18. Edwards, W., C.A. Lagadec, and D.K. Smith, *Solvent-gelator Interactions--using Empirical Solvent Parameters to Better Understand the Self-assembly of Gel-pHSAe Materials.* Soft Matter, 2011. **7**: p. 110-117.

19. Wang, R.Y., et al., *Architecture of Fiber Network: From Understanding to Engineering of Molecular Gels.* Journal of Physical Chemistry B, 2006. **10**: p. 25797-25802.

20. Li, J.L., et al., *Nanoengineering of a Biocompatible Organogel by Thermal Processing.* Journal of Physical Chemistry B, 2009. **113**(15): p. 5011-5015.

21. Liu, X.Y. and P.D. Sawant, *Determination of the Fractal Characteristic of Nanofiber-Network Formation in Supramolecular Materials.* CHEMPHYSCHEM, 2002. **4**: p. 374-377.

22. Huang, X., et al., *Distinct Kinetic Pathways Generate Organogel Networks with Contrasting Fractality and Thixotopic Properties.* Journal of the American Chemical Society, 2006(128): p. 15341-15352.

23. Terech, P., *Kinetics of Aggregation in a Steroid Derivative/Cyclohexane Gelifying System.* Journal of Colloid and Interface Science, 1985. **107**(1): p. 244-255.

24. Rogers, M.A. and A.G. Marangoni, *Non-Isothermal Nucleation and Crystallization of 12-Hydroxystearic Acid in Vegetable Oils.* Crystal Growth & Design, 2008. **8**(12): p. 4596-4601.

25. Lam, R.S.H. and M.A. Rogers, *Experimental Validation of the Modified Avrami Model for Non-Isothermal Crystallization Conditions.* Crystal Engineering Communications 2010. **13**: p. 866-875.

26. Rogers, M.A., A.J. Wright, and A.G. Marangoni, *Engineering the Oil Binding Capacity and Crystallinity of Self-assembled Fibrillar Networks of 12-Hydroxystearic Acid in Edible Oils.* Soft Matter, 2008. **4**(7): p. 1483-1490.

27. Rogers, M.A., A.J. Wright, and A.G. Marangoni, *Nanostructuring Fiber Morphology and Solvent Inclusions in 12-Hydroxystearic Acid/canola Oil Organogels (vol 14, pg 33, 2009).* Current Opinion in Colloid & Interface Science, 2009. **14**(3): p. 223-223.

28. Rogers, M.A., A.J. Wright, and A.G. Marangoni, *Nanostructuring Fiber Morphology and Solvent Inclusions in 12-Hydroxystearic Acid/canola Oil Organogels.* Current Opinion in Colloid & Interface Science, 2009. **14**(1): p. 33-42.

29. Menger, F.M., et al., *Chain-Substituted Lipids in Monomolecular Films. Effect of Polar Substituents on Molecular Packing.* Langmuir, 1989. **5**: p. 833-838.

30. Mallia, V.A., et al., *Robust Organogels from Nitrogen-Containing Derivatives of (R)-12-Hydroxystearic Acid as Gelators: Comparisons with Gels from Stearic Acid Derivatives.* Langmuir, 2009. **25**(15): p. 8615-8625.

31. Fameau, A.L., et al., *12-Hydroxystearic Acid Lipid Tubes under Various Experimental Conditions.* Journal of Colloid and Interface Science, 2010. **341**(1): p. 38-47.

32. Grahame, D.A.S., et al., *Influence of Chirality on the Modes of Self-Assembly of 12-Hydroxystearic Acid in Molecular Gels of Mineral Oil.* Soft Matter 2011. **7**: p. 7359-7365.

33. Huang, X. and R.G. Weiss, *Molecular Organogels of the Sodium Salt of (R)-12-Hydroxystearic Acid and Their Templated Syntheses of Inorganic Oxides.* Tetrahedron, 2007. **63**(31): p. 7375-7385.

34. Sakurai, T., et al., *A Comparative Study on Chiral and Racemic 12-Hydroxyoctadecanoic Acids in the Slutions and Aggregation States: Does the*

Racemic Form Really Form a Gel? Bulletin of the Chemical Society of Japan, 2010. **83**(2): p. 145-149.

35. Terech, P., et al., *Organogels and Areogels of Racemic and Chiral 12-Hydroxyoctadecanoic Acid.* Langmuir, 1994. **10**(10): p. 3406-3418.

36. Wright, A.J. and A.G. Marangoni, *Time, Temperature, and Concentration Dependence of Ricinelaidic Acid-canola Oil Organogelation.* Journal of the American Oil Chemists Society, 2007. **84**(1): p. 3-9.

37. Hansen, C.M., *Hansen Solubility Parameters*. 2nd ed. 2007, Boca Raton, Fl: CRC Press.

38. Marangoni, A.G., *Crystallography*, in *Fat Crystal Networks*, A.G. Marangoni, Editor. 2005, Marcel Dekker: New York. p. 1-20.

39. Sato, H. and S. Ueno, *Polymorphism in Fats and Oils*, in *Bailey's Industrial Oil and Fat Products*, F. Shahidi, Editor 2005, John Wiley & Sons, Inc: New York, USA. p. 77-120.

40. Lin-Vien, D., et al., *The Handbook of Infrared and Raman Characteristic Frequencies of Organic Molecules*. 1991, London, UK: Academic Press.

41. Rogers, M.A., T. Pedersen, and L. Quaroni, *Hydrogen-Bonding Density of Supramolecular Self-Assembled Fibrillar Networks Probed Using Synchrotron Infrared Spectromicroscopy.* Crystal Growth & Design, 2009. **9**(8): p. 3621-3625.

4.0 Nanoscale and Microscale Structural Changes Alter the Critical Gelator Concentration of Self-assembled Fibrillar Networks

J. Gao,[a] S. Wu,[a] T. J. Emge[b] and M. A. Rogers*[a]

a School of Environmental and Biological Sciences, Department of Food Science, Rutgers University; The State University of New Jersey, New Brunswick, NJ 08901

b School of Arts and Science, Department of Chemistry and Chemical Biology, Rutgers University; The State University of New Jersey; Piscataway, NJ 08854

**This chapter is published in published in *CrystEngComm* (DOI 10.1039/C3CE40323H), Received: 21 February 2013 / Accepted: 22 April 2013 / Published: 22 April 2013.

*Corresponding Author: Michael A. Rogers, Department of Food Science; Rutgers University; The State University of New Jersey, New Brunswick, NJ.
rogers@AESOP.Rutgers.edu

4.1 Abstract

It has been well established that self-assembled fibrillar networks require a meticulous balance between opposing molecular forces that control solubility and those intermolecular forces that direct epitaxial growth into axially symmetric elongated aggregates. The chemistry of the continuous phase (i.e., solvent) influences every level of structure in molecular gels. Solvent parameters induce low molecular weight gelators (LMOGs) to crystallize into different polymorphic forms, as well cause changes in the lamellar arrangement and domain size. These nanoscale alterations cause measureable differences in the microstructure, which induce physical macroscopic changes including the critical gelator concentration, melting temperature, melting enthalpy and opacity of the gel. Specifically, some solvents cause 12-hydroxystearic acid (12HSA) to self-assemble into triclinic parallel polymorphic forms where the lamellar spacing indicates that 12HSA forms an interdigitated network (lamellar spacing, 46 Å). The resulting molecular gels are opaque due to the presence of spherulitic crystals and have elevated critical gelator concentrations (i.e., greater than 1.5 wt%). Conversely, other solvents result in the formation hexagonal polymorphs and an extended bi-molecular length greater than 46 Å observed in the lamellar spacing. In these solvents, 12HSA forms translucent molecular gels, at concentrations less than 1.5 wt%, comprised of axially symmetric elongated crystals.

4.2 Introduction

Molecular organogels are thermally reversible, quasi-solid materials comprised of an organic liquid (usually ≥ 95 %) and a gelator molecule that self-assembles via physical interactions, including hydrogen-bonding,[1-4] π-π stacking,[5] dipole-dipole,[6, 7] and London dispersion forces,[8] into a 3-dimensional network.[9-11] Although the physical interactions between gelator molecules are central in understanding gelation, the solvent-gelator specific (i.e., H-bonding) and nonspecific (dipole-dipole, dipole-induced and instantaneous dipole induced forces) intermolecular interactions are equally important.[12, 13] The process of self-assembly, in molecular gels, is an intricate process that must balance the solubility and those intermolecular forces that control epitaxial growth into axially symmetric elongated aggregates.[10, 13-16] During assembly, individual molecules are driven to assemble by molecular self-recognition and intermolecular non-covalent interactions into oligomers and subsequently, these oligomers assemble into fibrillar aggregates immobilizing the solvent via capillary forces.[17, 18]

12HSA, a structurally simple, highly effective LMOG has been studied extensively.[2, 3 ,15, 19-32] Critical interactions between the solvent and 12HSA govern the physical behavior and gelation process.[12] Self-assembly begins, in LMOGs, after a critical concentration is achieved, below which the gelator is soluble existing primarily as monomers in solution.[12] After sufficient addition of gelator molecules, the critical concentration is reached and gelation begins, leading to a decrease in the concentration of gelator in the solution phase.[12] Further addition of gelator molecules cause the solvent to be immobilized but that does not alter the soluble concentration of gelator

molecules.[12] Since gelator solubility is dependent on the nature of the solvent, most studies stop at correlating critical gelator concentration (CGC) to solubility parameters.[12, 13]

Reports by Gao et al.,[13] and Yan et al.,[33] have both shown that the CGC increases as the polar and hydrogen-bonding Hansen solubility parameters (HSP) increase irrespective of the gelator chemistry. A recent report went beyond the CGC effects and found solvents modify interactions between pyrenyl group interactions in pyrenyl-linker-glucono gelators.[33] In this current work, we use 12-hydroxystearic acid to study the nanostructure and microstructure of the gels in different solvents with CGC's varying between 0.2 to 2.5 wt%.

4.3 Method

Solvent selection criteria were maintained as simply as possible with the aliphatic chain being linear, saturated, the functional group located in the primary position and the solvent must be in a liquid state between 10 and 30 ^{o}C. The only exceptions to these selection criteria were the ethers and ketones where the functional group was located in the exact middle of the molecule. Apolar solvents included the aliphatics, polar solvents were subdivided into four categories: aldehydes, ketones, ethers and nitriles; as well, the solvents capable of hydrogen bonding were divided into two groups; thiols and amines (Table 1). All solvents and D-12-hydroxystearic acid (12HSA) were obtained from Sigma-Aldrich (Cherry Hill, NJ, USA) with purity greater than 0.95%.

4.3.1 Sample Preparation and Gel Test

12HSA was dispersed in 2 ml of solvent in 4 ml glass vials capped with PTFE lined lids (VWR, Randor, PA). 12HSA was studied in numerous solvents (Table 1) and

the concentration was studied at 0.1% increments from 0.1 wt% to 3 wt%. After 12HSA was dispersed in each solvent and was capped, the vials were placed in a hot water bath set at 95 ^{o}C for 20 min. After the sol appeared clear, it was removed and stored for 24 hours at 20 ^{o}C in the chemical fume hood. To determine if the material was a gel, the vial was inverted for 1 hour and if the material did not flow it was considered gelled. This method had to be employed due to the extremely high volatility of several of the solvents employed.

4.3.2 Free Induction Decay-NMR Measurements

Samples of 2 wt% 12HSA in various solvents were subjected to T_2 relaxation measurements on a Bruker mq20 Series NMR Analyzer (Bruker, Milton, Ontario, Canada). A Hahn-echo pulse sequence was used to measure the Free Induction Decay (FID). The operational pulse length was obtained using the calibration procedures recommended by the manufacturer. The 90^{o} pulse was 2.6 μs and the 180^{o} pulse was 5.1 μs. This allowed determination of the gain (64) and recycle delay (5 s). Tau was selected to be as short as possible (0.5 ms) to minimize chemical exchange and diffusion effects on the decay curves.

4.3.3 Differential Scanning Calorimetry

10 to 12 mg samples of 2 wt% 12HSA in various organic solvents were transferred into Alod-Al hermetic DSC pans. The DSC chamber (Q2000, TA instruments, New Castle, DE) was pre-cooled to 20 ^{o}C before the sample was placed into the chamber which was continually flushed with nitrogen (0.5 ml min^{-1}). The samples were heated to 90 ^{o}C and cooled to 20 ^{o}C at 2 ^{o}C min^{-1} to determine the peak crystallization and melting

temperatures. The enthalpy of melt was determined by integrating the endothermic transition using the software's tangent skimming method.

4.3.4 Microscopy

The supramolecular structure of 2 wt% 12HSA in various solvents was imaged using a Linkham Imagining station (Linkham, Surrey, England) equipped with a Q imagining 2560 × 1920 pixel CCD camera (Micropublisher, Surrey, Canada) and a 10X Olympus lens (0.25 N.A.) (Olympus, Tokyo, Japan). Samples were placed on a glass slide and a cover slip was placed on top of the sample. The slide was transferred into a Peltier temperature control stage (LTS120, Linkham, Surrey, England) using a water reservoir as the heat sink. The samples were heated to 80 ^{o}C and cooled at 2 ^{o}C min^{-1} to 20 ^{o}C to observe fiber formation using non-polarized light. Light micrographs were calibration with a 100 μm micrometer.

4.3.5 Fourier Transform Infrared Spectroscopy

A small portion of 2 wt% has gel was removed directly from the glass vial after 24 hours of storage and was placed directly on the Attenuated total refraction (ATR) prism in a Thermo Nicolet FT-IR (Thermo Fisher Scientific, MA, USA). 256 scans were collected at a resolution of 4 cm^{-1} using an empty cell as the background for the FT-IR measurements. The carbonyl (~1700 cm^{-1}) and hydroxyl (~3200 cm^{-1}) signals were measured.

4.3.6 X-ray Diffraction

2 wt% 12HSA gels were loaded into 0.5 mm silica capillaries and were flame sealed. The capillaries, containing sample, were placed into an Enraf-Nonius FR571 rotating anode X-ray generator equipped with Rigaku Osmic mirror optic system (~0.06

deg 2*q* nominal dispersion for Cu Ka; λ = 1.5418 Å) and a Bruker HiStar area detector operating at 40 kV and 40 mA. The X-ray diffraction (XRD) or wide-angle X-ray scattering (WAXS) patterns of 12HSA gels were collected at room temperature over a period of 300 s. The sample to detector distance was 10.0 cm and the standard spatial calibration was performed at that distance. Scans were 4 degrees wide in omega (*w*) with fixed detector, or Bragg angle (2*q*) of 0 deg, and fixed platform (*f* and *c*) angles of 0 and 45 deg, respectively. In all cases, the count rate for the area detector did not exceed 100 000 cps.

4.4 Discussion

The CGC of 12HSA varies between 0.2 wt% and 2.5 wt% depending on the solvent used as the continuous phase (Table 1).[13] The CGC, using the selected solvents, had to be determined using the tube inversion method due to the extreme solvent volatility. However, this technique and similar techniques (‘‘falling ball’’ method) have been employed previously to determine the CGC of molecular gels.[13,26,33,34] It is not surprising that modifying the chemistry of the solvent modifies the CGC, as it has previously been reported that solvent parameters influence the supramolecular structure of LMOGs. The presence or absence of solvent gelator interaction may induce changes in the fiber thickness, the number of junction zones between fibers and the sense of helical twist within the fiber.[12,18] These changes have been shown to not only modify the CGC of 12HSA molecular gels but they also alter the opacity.[13] Apart from observing the CGC and the gel opacity few structure-function mechanisms between solvent structure and gelator have been studied.[33]

Table 1: Critical gelator concentration determined using the inverted vial technique for the studied solvents and the acronym use to identify the points on individual figures.

Solvent	Acronym	CGC (wt%)
Hexane	**6-ane**	**0.4**
Heptane	**7-ane**	**0.3**
Octane	**8-ane**	**0.3**
Nonane	**9-ane**	**0.25**
Decane	**10-ane**	**0.2**
Dodecane	**12-ane**	**0.2**
Octanal	**8-al**	**2.5**
Nonanal	**9-al**	**2.5**
Decanal	**10-al**	**1.6**
4-Heptone	**7-one**	**2.4**
5-Nonanone	**9-one**	**2.1**
6-Undecanone	**11-one**	**1.6**
Dipropyl ether	**7-eth**	**2.2**
Dibutyl ether	**9-eth**	**1.5**
Dipentyl ether	**11-eth**	**1.4**
Ethanenitrile	**2-nit**	**2.3**
Propanenitrile	**3-nit**	**2.3**
Butanenitrile	**4-nit**	**2.1**
Octanenitrile	**6-nit**	**1.5**
Nonanenitrile	**9-nit**	**0.9**
1-Pentanethiol	**5-thi**	**0.5**
1-Hexanethiol	**6-thi**	**0.45**
1-Heptanethiol	**7-thi**	**0.45**
1-Octanethiol	**8-thi**	**0.4**
1-Decanethiol	**10-thi**	**0.3**

In the case of 12HSA, the molecular gel is comprise of self-assembled fibrillar networks (SAFiN) driven to assemble by enthalpic forces forming a network of crystalline fibers.[10] The crystalline nature of the fibers has resulted in numerous research groups developing and applying crystallographic mismatch theory to molecular gels.[2,24,35–37] Structural features that effect crystal perfection include: crystallographic mismatches, solvent inclusions, different polymorphic forms and high crystal surface area to volume ratios. The “degree of crystallinity” can be probed using

the T_2 relaxation and amplitude obtained using a free induction decay (FID) pulse sequence coupled with pulsed nuclear magnetic resonance (pNMR) (Figure 4-1 A and 4-1 B) or using the onset of the melting (Figure 4-2 B and 4-2 C) and enthalpy of the transition (Figure 4-2 D and 4-2 E) determined using DSC.

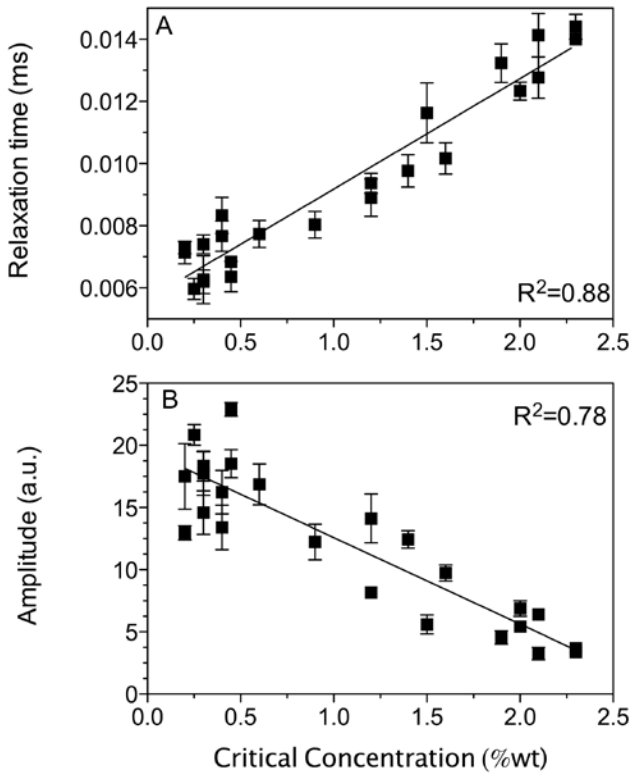

Figure 4-1: Pulse NMR proton free induction decay relaxation times (A), decay amplitudes (B) for 2 wt% 12-hydroxystearic acid molecular gels in various organic solvents.

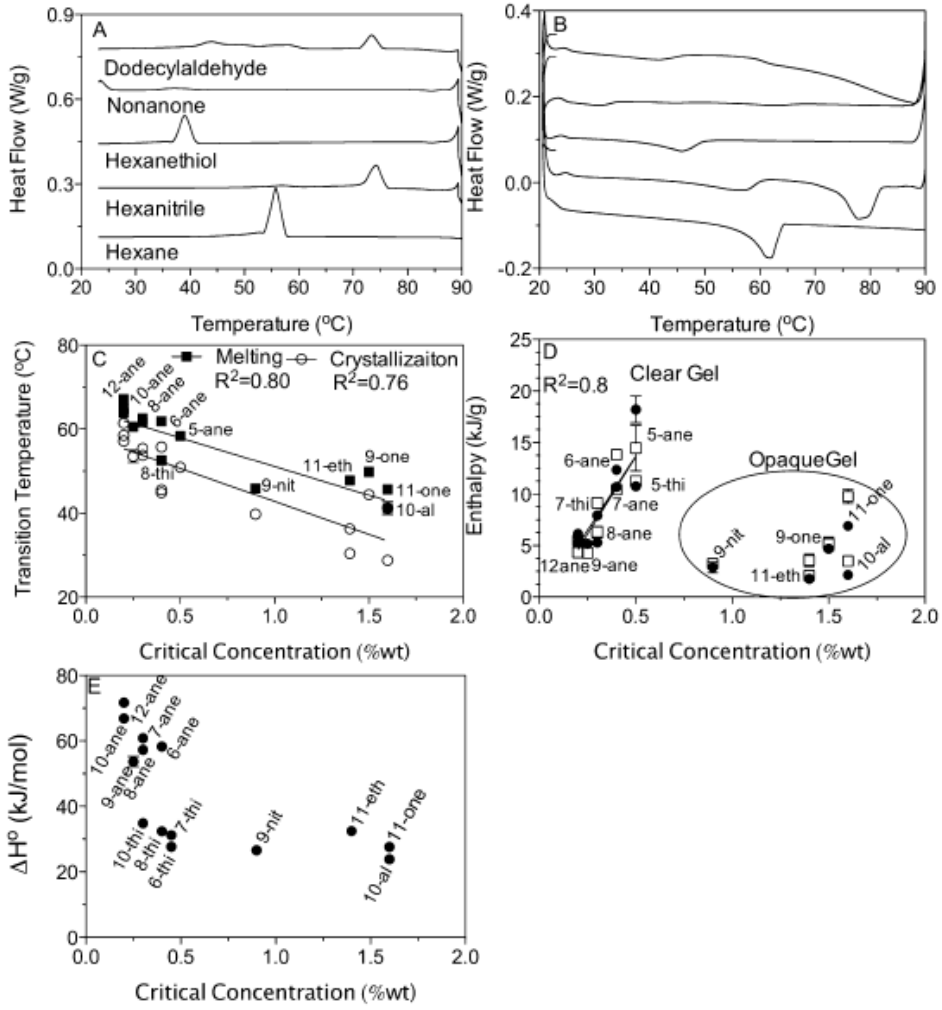

Figure 4-2: DSC thermograms of the exothermic crystallization (A) and endothermic melting transition (B) of 12HSA molecule gels. Crystallization and melting temperatures (C) and melting enthalpies obtained by integration of the thermograms (D) and the Hildebrand solubility equation (E) for 12HSA molecular gels in several organic solvents.

T_2 relaxations, below 70 μs, are proportional to the perfection of the crystalline phase.[30,31] A high degree of 'crystallinity' is correlated to shorter T_2 free induction times[38] and relates to numerous structural features of crystals suspended in solvents. For 12HSA, a positive linear correlation was found between the T_2 relaxation time and the CGC (Figure 4-1 A). Although this suggests that as the CGC increases there is a decrease in the crystal perfection; the nature of the crystal imperfections cannot be

elucidated using this technique. For example, the decrease in crystal perfection may be related to several structural changes such as: different polymorphic forms, the number of solvent inclusions, the amount of interfacial area between the 12HSA and solvent, or any combination thereof.

The T_2 decay amplitude, obtained from the FID provides additional useful information regarding the crystalline nature of the SAFiNs (Figure 4-1 B). A negative correlation between the T_2 amplitude CGC is observed (Figure 4-1 B). This suggests that as the CGC increases, the solubility of the gelator also increases resulting in less crystalline mass. As the solvent conditions change (i.e., increasing polar and hydrogen bonding Hansen solubility parameters), the CGC increase to a point, after which 12HSA becomes soluble in the solvent and corresponds to a T_2 FID decay amplitude at or near zero.

The onset of the melting temperature (Figure 4-2 B and 4-2 C) is also related to the degree of crystalline order. In polymer systems, a decrease in Tm is observed upon the addition of a solvent, which acts as a plasticizer.[39] A decrease in the melting temperature is associated with an increase in the surface area associated with the crystalline phase of the molecular gel; therefore, changes in the melting temperature may be explained using Gibbs free-energy curves.[23] For 12HSA, the CGC was negatively correlated with the crystallization and melting temperature (Figure 4-2 C). This signifies that an increase in the CGC corresponds to a decrease in the crystal size and/or more imperfect crystals are present.[39] Comparing the onset of melt (Figure 4-2 A and 4-2 C) and the relaxation time (Figure 4-1 A) both indicate a decrease in the ‘crystallinity’ with increasing CGC. The enthalpy of the transition may be attained by integrating the DSC

thermograms (Figure 4-2 D) as well as by using the Hidebrand solubility parameter (Figure 4-2 E), which is derived from Van't Hoff equation using the onset temperature of melting:[40]

$$\log_{10} x = \frac{\Delta H}{R} \left(\frac{1}{T_{\mathrm{m}}} - \frac{1}{T}\right)$$

where x represents the mol fraction of the higher melting component, ΔH is the enthalpy of melt for the higher melting component, R is the universal gas constant, and T_{m} and T are the melting temperatures of the higher melting fraction and the gel, respectively. The enthalpy of melt, determined by integrating the DSC thermograms, increased as a CGC increases and then drastically decreases once the CGC reached ~1.0 wt% (Figure 4-2 D). The increase in the enthalpy, below 1 wt%, contradicts observations made using pNMR, which suggest that the amount of crystalline materials decreases as CGC increases (Figure 4-1B). This contradiction, along with previous observations that the gels undergo a transition from a translucent to an opaque gel at CGCs at ~1 wt%,[13] were used to formulate the hypothesis that the molecular arrangement of 12HSA differs in dissimilar solvents giving rise to different intermolecular non-covalent interactions causing a drastic modification in the macroscopic properties of the gel. Hence, the amount of energy released during the phase transition is a function of both the amount of crystalline mass and also the nature of the non-covalent interactions between 12HSA molecules.

In order to more accurately probe the solubility issues of the 12HSA gels the enthalpy was calculated using the Hildebrand solubility equation. Using this method, the enthalpy is determined based on the chemical equilibrium at a specific temperature. This suggests that the enthalpy will be solely a measure of the amount of crystalline 12HSA

molecules. The enthalpy of melt, determined using the Hildebrand solubility equation was negatively correlated with the CGC (Figure 4-2 E) corresponding to the observations made using the T_2 relaxation amplitude (Figure 4-1 B).

The difference between 12HSA gels in different solvents measured using pNMR and DSC, along with previous observations in the visual opacity compelled the examination of microstructure and nanostructure. To probe the microstructure of 12HSA gels brightfield microscopy was employed (Figure 4-3). CGC, less than 1 wt%, assembled into axially symmetric elongated aggregates radiating from central nuclei. These fibers are only a few microns in width but may exceed 100 μm in length (Figure 4-3, top row). The lack of junction zones and narrow fiber width cause them to appear transparent because the structural units an incapable of diffracting light. At low CGCs thin fibers are observed; however, as the CGC increases there is a transition to dense clusters of fibers and eventually to spherulitic structures. The transition from fibril aggregates to spherulitic crystals, in molecular gels, arises due to crystallographic mismatches.[35,36] These crystal imperfections which lead to the generation of spherulitic crystals coincides with the reduced ‘crystallinity’ observed using pNMR and DSC which confirms in part that the molecular arrangement of 12HSA differs in dissimilar solvents giving rise to different intermolecular non-covalent interactions.

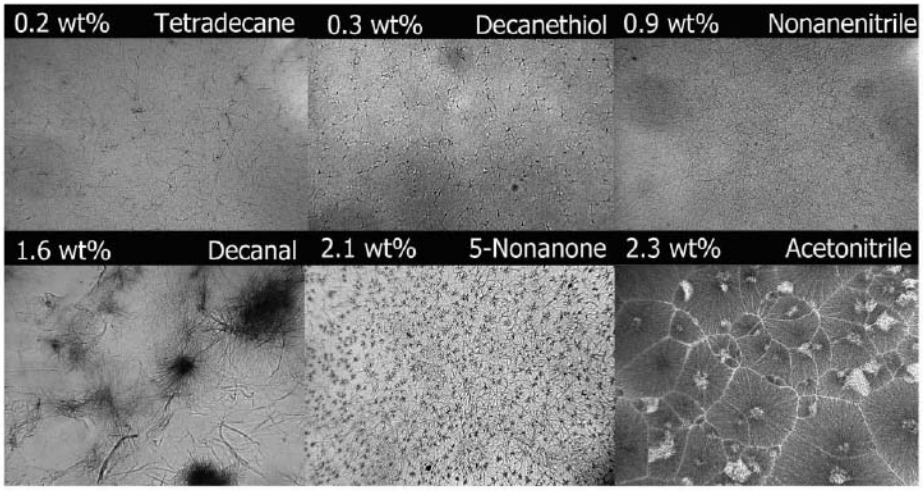

Figure 4-3: Light micrographs of 2 wt% 12-hydroxystearic acid organogels in different organic solvents. Critical gelator concentration of 12-HSA in each solvent is displayed in upper left corner. Width of micrograph is 120 μm.

The changes in the supramolecular structure provide some clarification to the decrease in the crystalline order measured using the relaxation time and amplitude (Figure 4-1 A), and the enthalpy of melt and onset of melt (Figure 4-2). However, as the CGC increases, the major changes to the supramolecular 12HSA network structure must be driven either due to a cocrystallization of the gelator and solvent or different molecular packings within the crystal occur. The non-covalent interactions between 12HSA molecules (Figure 4-4) and the molecular arrangements (Figure 4-5) were studied using FT-IR and XRD.

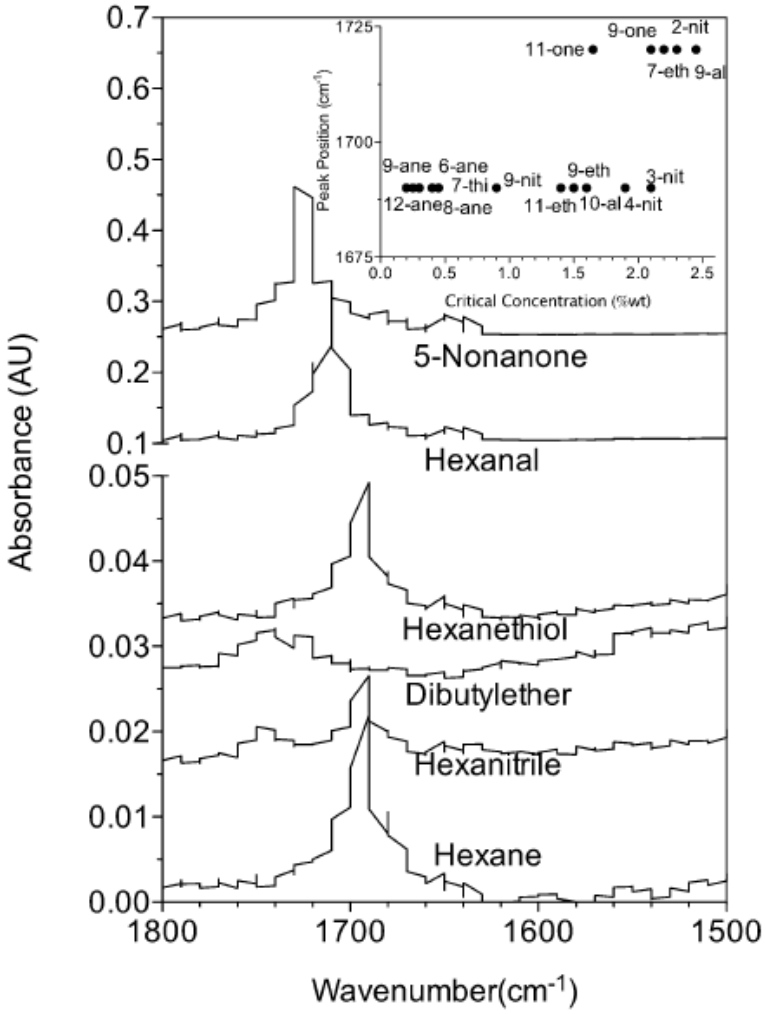

Figure 4-4: Vertically offset FT-IR spectra focusing on the carboxylic acid region of 12HSA molecular gels in various solvents using the air as the background. (Inset: FT-IR carboxylic acid peak position of 2.5 wt% 12HSA molecular gels in various solvents as a function of CGC.)

Using FT-IR, 12HSA has been shown to form carboxylic acid dimers and the longitudinal growth is driven by interactions between the 12 hydroxyl groups between adjacent molecules.[1,41] Cyclic dimers have a peak position at 1690 cm^{-1} while free monomers appear at 1720 cm^{-1} (Figure 4-4). When the critical concentration is less than 1.5 wt%, 12HSA is able to form dimers and above 1.5 wt%, depending on the solvent; 12HSA can either exist as monomers or dimers (Figure 4-4, insert). The existence of

12HSA monomers corresponds to a lower enthalpy of melt and crystallization due impart to fewer physical bonds in the network structure (Figure 4-2).

Structural changes were also probed using XRD (Figure 4-5). In general, the 001 and higher order 003 peaks could be resolved (Figure 4-5A). However, no obvious changes were observed with the exception of the aldehydes, which had a very broad 001 peak. The wide-angle spacings showed much more deviation between samples (Figure 4-5 B). Some solvents exhibited a hexagonal sub cell spacing (~4.3 Å) while others showed a triclinic parallel sub cell (strong peak at 4.6 Å, and two weak peaks at 3.9 Å and 3.8 Å) (Figure 4-5 B) which has been previously shown.[42] The d spacing of the 001 wide-angle spacing was plotted as a function of CGC and an inverse correlation was observed (Figure 4-5 C). At low CGCs the d-spacing was slightly longer than the bimolecular length of 12HSA, while at CGCs greater than ~1.5 wt% the d-spacing was shorter than the bimolecular length of 12HSA. This supports the observation that when cyclic dimers form, the d-spacing must exceed the extended bimolecular length. However, if 12HSA does not effectively form a dimer then the d-spacing may be less than the bimolecular length suggesting interdigitation of 12HSA in the crystals. Along with the change to the carboxylic head group and the bimolecular length, a polymorphic transition was also observed. Low CGCs correspond to hexagonal sub cell spacing and above 1.5 wt% the triclinic parallel sub cell spacing is observed (Figure 4-5 D).

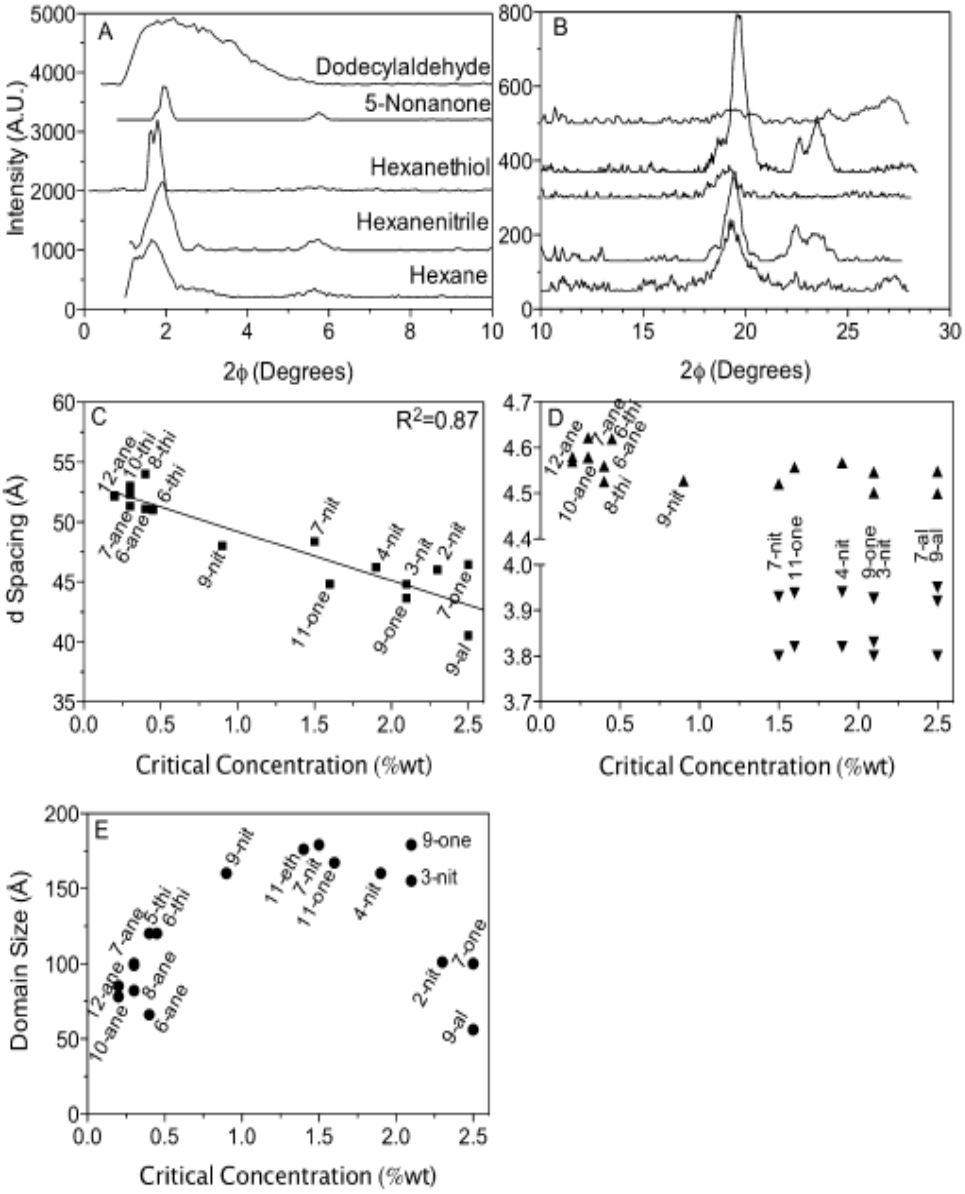

Figure 4-5: Vertically offset wide-angle (A) and short-angle (B) diffractograms for 12HSA in various solvents. The long (C) and short spacings (D) obtained from XRD and the domain size (E) calculated using the Williamson Hull equation for 12HSA molecular gels as a function of CGC.

The full width half max for each peak was obtained and using a Williamson Hull equation the domain size was obtained. The Williamson Hull equation is: [43]

$$\mathrm{FW}(S)x\cos(\theta) = \frac{K\lambda}{\mathrm{size}} + \ (4(\mathrm{strain})\sin(\theta))$$

where FW is the full-width half-max, θ is the diffraction angle, K is the Scherrer constant, λ is the x ray wavelength. The Williamson Hull plots FW(S)xcos(θ) *versus* sin(θ). Since few diffraction peaks were observed we had to assume that there was no strain and hence the slope was set equal to zero. From the y-intercept, the domain size was calculated and plotted against the CGC (Figure 4-5 E). The domain size follows a parabolic shape when plotted against the CGC. The vertex of the parabola corresponds to a transition from the hexagonal sub cell to the triclinic parallel sub cell. As the CGC increases from 0.2 to 1.5 wt% (corresponding with an increase in the δ_p and δ_h) the solvent properties causes an increase in the domain size. At CGCs greater than 1.5 wt%, the domain size decreases as the CGC increases.

What is astonishing about this study is solvent not only effects final physical properties and macroscopic appearance of the gel but also the microscopic structure and nanostructure (Figure 4-6). In molecular gels, the solvent structure is as important as the gelator structure when trying to understand how and why certain compounds are capable of self-assembling into axially symmetric elongated aggregates capable of entraining hundreds if not thousands of solvent molecules per gelator molecule.

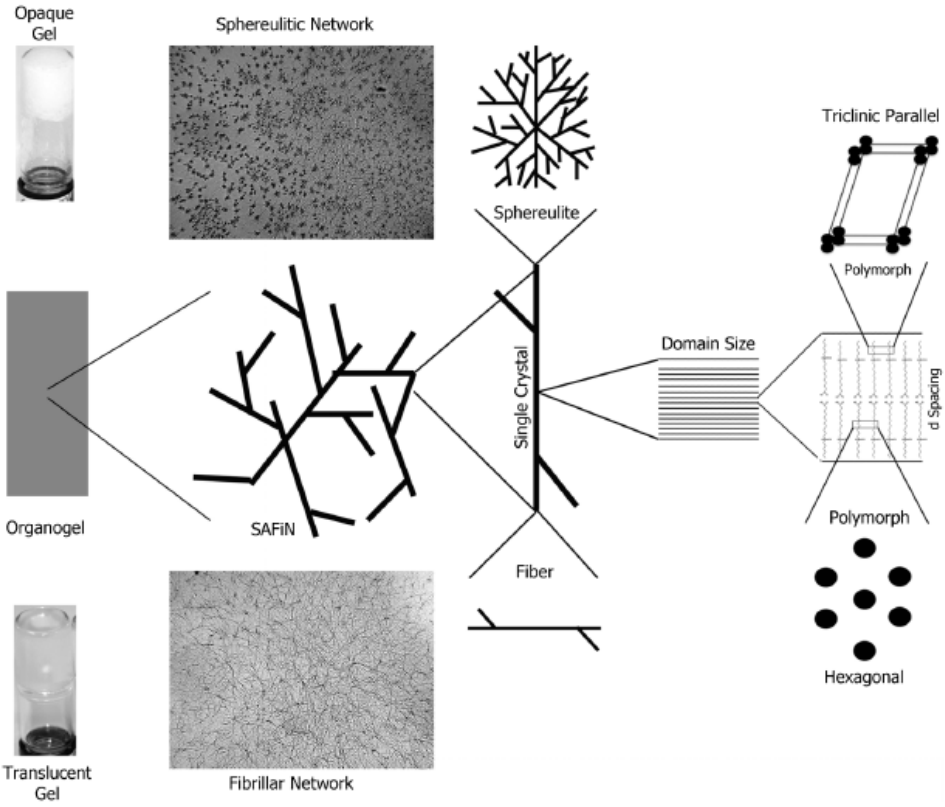

Figure 4-6: Different levels of structure examined in this structure which are effected by the solvent properties and CGC.

4.5 Conclusions

Modifying the solvent in molecular gels effects the CGC, physical properties of the gels and the opacity. The CGC changes because of changes in the gelator solubility, altered polymorphic crystal forms, and microscopic changes in the network structure. For 12HSA, solvents that require concentrations greater than 1.5 wt% to form molecular gels have spherulitic crystals, a triclinic parallel polymorphic form and the 12HSA molecules are interdigitated. Conversely, translucence gels at concentrations less than 1.5 wt% result from the formation of a fibrillar crystal network, with a hexagonal polymorph and the d spacing is greater than the bimolecular length.

4.6 Works Cited

1. Kuwahara, T., et al., *Crystal Structure of DL-12-Hydroxystearic Acid.* Chemistry Letters, 1996. **25**: p. 435-436.

2. Lam, R., et al., *A Molecular Insight into the Nature of Crystallographic Mismatches in Self-assembled Fibrillar Networks under Non-isothermal Crystallization Conditions.* Soft Matter, 2010. **6**(2): p. 404-408.

3. Li, J.L., et al., *Arichitecture of a Biocompatible Supramolecular Material by Supersaturation-Driven Fabrication of its Network.* Journal of Physical Chemistry B, 2005. **109**: p. 24231-24235.

4. Rogers, M.A., et al., *Multicomponent Hollow Tubules Formeed Using Phytosterol and γ-Oryzanol-Based Compounds: An Understanding of Their Molecular Embrace.* Journal of Physical Chemistry, 2010. **114**: p. 8278-8295.

5. Moffat, J.R. and D.K. Smith, *Controlled Self-Sorting in the Assembly of 'Multi-Gelator' Gels.* Chemical Communication, 2009. **3**: p. 316-318.

6. Brotin, T., J.P. Devergne, and F. Fages, *Photostationary Fluorescence Emission and Time Resoved Spectroscopy of Symmetrically Disubstituted Anthracenes on teh meso and Side Rings: The Unusual Behavior of the 1,4 Derivative.* Photochemistry and Photobiology, 1992. **55**: p. 349-358.

7. Terech, P., I. Furman, and R.G. Weiss, *Structures of Organogels Based Upon Cholesteryl 4-(2-Anthryloxy)Butanoate, A Highly Efficient Luminescing Gelator - Neutron AND X-Ray Small-Angle Scattering Investigations.* Journal of Physical Chemistry, 1995. **99**(23): p. 9558-9566.

8. Toro-Vazquez, J.F., et al., *Relationship Between Molecular Structure and Thermo-mechanical Properties of Candelilla Wax and Amides Derived from (R)-12-Hydroxystearic Acid as Gelators of Safflower Oil.* Food Biophysics, 2010. **5**(3): p. 193-202.

9. Mallia, V.A., et al., *Reversible Phase Transitions within Self-Assembled Fibrillar Networks of (R)-18-(n-Alkylamino)octadecan-7-ols in Their Carbon Tetrachloride Gels.* Journal of the American Chemical Society, 2011. **133**: p. 15045-15054.

10. Weiss, R.G. and P. Terech, *Introduction*, in *Molecular Gels: Materials with Self-Assebled Fibrillar Networks*, R.G. Weiss and P. Terech, Editors. 2006, Springer: Dordrecht, The Neatherlands. p. 1-13.

11. George, M. and R.G. Weiss, *Molecular Organogels. Soft Matter Comprised of Low-Molecular-Mass Organic Gelators and Organic Liquids.* Accounts of Chemical Research, 2006. **39**: p. 489-497.

12. Zhu, G. and J.S. Dordick, *Solvent Effect on Organogel Formation by Low Molecular Weight Molecules.* 2006. **18**(Chemistry of Materials): p. 5988-5995.

13. Gao, J., S. Wu, and M.A. Rogers, *Harnessing Hansen Solubility Parameters to Predict Organogel Formation.* Journal of Materials Chemistry, 2012. **22**: p. 12651-12658.

14. Suzuki, M., et al., *Effects of Hydrogen Bonding and van der Waals Interactions on Organogelation Using Designed Low-molecular-weight Gelators and Gel Formation at Room Temperature.* Langmuir, 2003. **19**(21): p. 8622-8624.

15. Rogers, M.A. and A.G. Marangoni, *Solvent-Modulated Nucleation and Crystallization Kinetics of 12-Hydroxystearic Acid: A Nonisothermal Approach.* Langmuir, 2009. **25**(15): p. 8556-8566.

16. Raynal, M. and L. Bouteiller, *Organogel Formation Rationalized by Hansen Solubility Parameters.* Chemical Communication, 2011. **47**: p. 8271-8273.

17. Hardy, J.G., A.R. Hirst, and D.K. Smith, *Exploring Molecular Recognition Pathways in One- and Two-component Gels Formed by Dendritic Lysine-based Gelators.* Soft Matter, 2012. **8**: p. 3399-3406.

18. Edwards, W., C.A. Lagadec, and D.K. Smith, *Solvent-gelator Interactions--Using Empirical Solvent Parameters to Better Understand the Self-assembly of Gel-phase Materials.* Soft Matter, 2011. **7**: p. 110-117.

19. Terech, P., *Kinetics of Aggregation in a Steroid Derivative/Cyclohexane Gelifying System.* Journal of Colloid and Interface Science, 1985. **107**(1): p. 244-255.

20. Rogers, M.A. and A.G. Marangoni, *Non-Isothermal Nucleation and Crystallization of 12-Hydroxystearic Acid in Vegetable Oils.* Crystal Growth & Design, 2008. **8**(12): p. 4596-4601.

21. Lam, R.S.H. and M.A. Rogers, *Experimental Validation of the Modified Avrami Model for Non-Isothermal Crystallization Conditions.* Crystal Engineering Communications 2010. **13**: p. 866-875.

22. Li, J.L., et al., *Nanoengineering of a Biocompatible Organogel by Thermal Processing.* Journal of Physical Chemistry B, 2009. **113**(15): p. 5011-5015.

23. Rogers, M.A., A.J. Wright, and A.G. Marangoni, *Engineering the Oil Binding Capacity and Crystallinity of Self-assembled Fibrillar Networks of 12-Hydroxystearic Acid in Edible Oils.* Soft Matter, 2008. **4**(7): p. 1483-1490.

24. Wang, R.Y., et al., *Architecture of Fiber Network: From Understanding to Engineering of Molecular Gels.* Journal of Physical Chemistry B, 2006. **10**: p. 25797-25802.

25. Menger, F.M., et al., *Chain-Substituted Lipids in Monomolecular Films. Effect of Polar Substituents on Molecular Packing.* Langmuir, 1989. **5**: p. 833-838.

26. Mallia, V.A., et al., *Robust Organogels from Nitrogen-Containing Derivatives of (R)-12-Hydroxystearic Acid as Gelators: Comparisons with Gels from Stearic Acid Derivatives.* Langmuir, 2009. **25**(15): p. 8615-8625.

27. Fameau, A.L., et al., *12-Hydroxystearic Acid Lipid Tubes under Various Experimental Conditions.* Journal of Colloid and Interface Science, 2010. **341**(1): p. 38-47.

28. Grahame, D.A.S., et al., *Influence of Chirality on the Modes of Self-Assembly of 12-Hydroxystearic Acid in Molecular Gels of Mineral Oil.* Soft Matter 2011. **7**: p. 7359-7365.

29. Huang, X. and R.G. Weiss, *Molecular Organogels of the Sodium Salt of (R)-12-Hydroxystearic Acid and Their Templated Syntheses of Inorganic Oxides.* Tetrahedron, 2007. **63**(31): p. 7375-7385.

30. Sakurai, T., et al., *A Comparative Study on Chiral and Racemic 12-Hydroxyoctadecanoic Acids in the Slutions and Aggregation States: Does the Racemic Form Really Form a Gel?* Bulletin of the Chemical Society of Japan, 2010. **83**(2): p. 145-149.

31. Terech, P., et al., *Organogels and Areogels of Racemic and Chiral 12-Hydroxyoctadecanoic Acid.* Langmuir, 1994. **10**(10): p. 3406-3418.

32. Wright, A.J. and A.G. Marangoni, *Time, Temperature, and Concentration Dependence of Ricinelaidic Acid-canola Oil Organogelation.* Journal of the American Oil Chemists Society, 2007. **84**(1): p. 3-9.

33. Yan, N., et al., *Pyrenyl-linker-glucono Gelators. Correlations of Gel Properties with Gelator Structures and Characterization of Solvent Effects*. Langmuir, 2013. **5**: p. 793–805.

34. Wu, Y., et al., *Solvent Effects on Structure, Photoresponse and Speed of Gelation of a Dicholesterol-linked Azobenzene Organogel*. Soft Matter, 2011. **7**: p. 9177–9183.

35. Liu, X.Y. and P.D. Sawant, *Determination of the Fractal Characteristic of Nanofiber-network Formation in Supramolecular Materials*. ChemPhysChem, 2002. **4**： p. 374–377.

36. Liu, X.Y. and P.D. Sawant, *Mechanism of the Formation of Self-organized Microstructures in Soft Functional Materials*. Adv. Mater., 2002. **14**: p. 421–426.

37. Wang, R.Y., et al., *From Kinetic-structure Analysis to Engineering Crystalline Fiber Networks in Soft Materials*. Phys. Chem., 2013. **15**: p. 3313–3319.

38. Duval, F.P., J.P.M. van Duynhoven, and A. Bot, *Practical Implications of the Phasecompositional Assessment of Lipid-based Food Products by Time-domain NMR*. J. Am. Oil Chem. Soc., 2006. **83:** p. 905–912.

39. Farbi, D., J. Guan, and A. Cesaro, *Crystallisation and Melting Behaviour of Poly (3-hydroxybutyrate) in Dilute Solution: Towards an Understanding of Physical Gels*. Thermochim. Acta, 1998. **321**: p. 3–16.

40. Wesdorp, L.H. et al., *Phase Equilibria in Fat*, in *Fat Crystal Networks*, A. G. Marangoni, Editor. 2005, Marcel Dekker: New York, USA.

41. Lin-Vien, D. et al., *The Handbook of Infrared and Raman Characteristic Frequencies of Organic Molecules*. Academic Press, London, UK, 1991.

42. Wu, S. et al., *Solvent Induced Polymorphic Nanoscale Transitions for 12-Hydroxyoctadecanoic Acid Molecular Gels*. Cryst. Growth Des., 2013. **13**: p. 1360–1366.

43. Lou, D. and N. Audebrand, *Profile Fitting and Diffraction Line-Broadening Analysis, Advances in X-ray Diffraction*, 1997. **41**: p. 556–565.

5.0 Conclusion

Solvents that have different functional group and aliphatic chain lengths affect the CGC, physical properties of the gels and the opacity. The CGC changes in part due to changes in the gelator solubility in the solvent but also due to altered polymorphic crystal forms and microscopic changes in the network structure. For 12HSA, solvents (i.e., nitriles, aldehydes, and ketones) that require concentrations greater than 1.5 wt% to form molecular gels have spherulitic crystals, a triclinic parallel polymorphic form (~ 4.6, 3.9, and 3.8 Å) and the 12HSA molecules are interdigitated in the lamellar form. Conversely, translucence gels at concentrations less than 1.5 wt% (i.e., alkanes and thiols) result from the formation of a fibrillar crystal network, with a hexagonal polymorph (~4.1 Å) and the distance between lamella are greater than the bi-molecular length of 12HSA. This is the first report of modifying the polymorphic forms by varying the solvents utilized, which provides another degree of tailor ability for molecular gels. This knowledge will allow new and improved functionalities which can be manipulated by the chemist to control the physical properties of the gel.

6.0 Appendices

Appendix 1

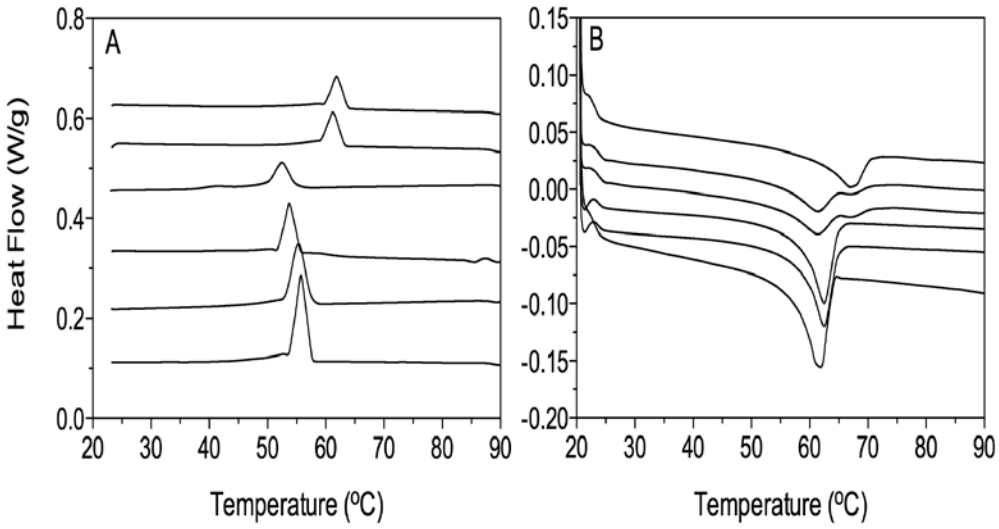

A) DSC thermograms of the exothermic crystallization of 12HSA molecule gels. The diffractrograms from bottom to the top are hexane, heptane, octane, nonane, decane, dodecane, tetradecane.

B) DSC thermograms of the endothermic melting transition of 12HSA molecule gels. The diffractrograms from bottom to the top are hexane, heptane, octane, nonane, decane, dodecane, tetradecane.

Appendix 2

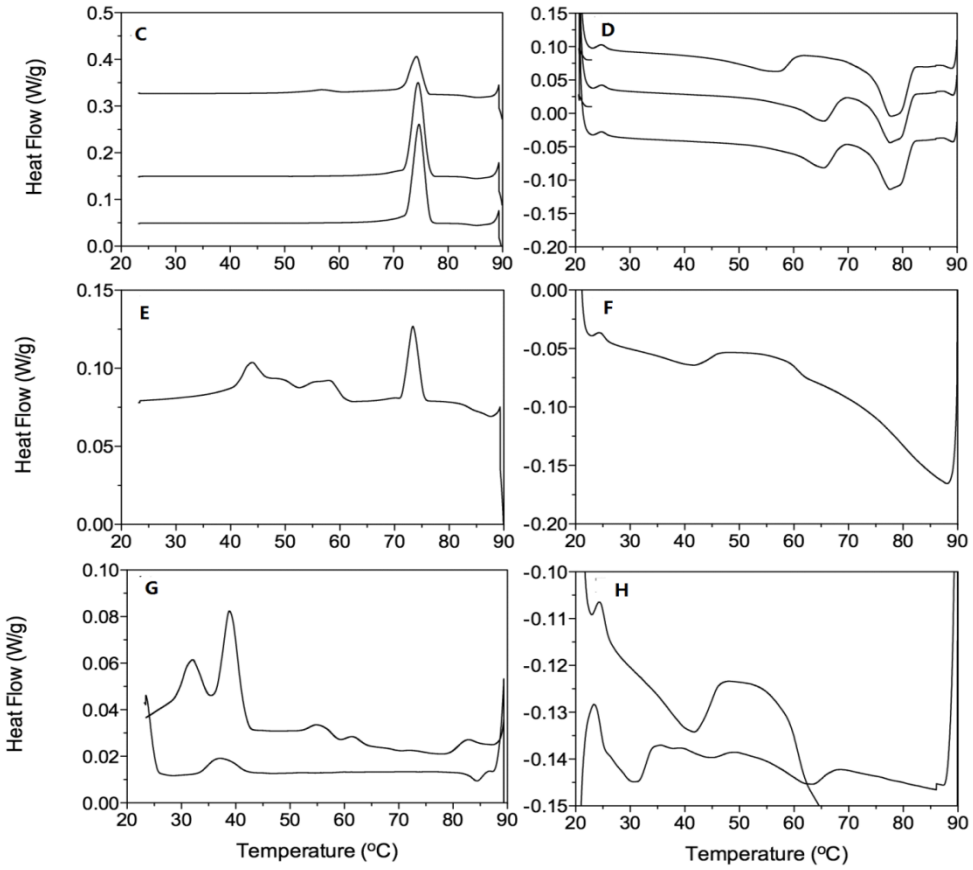

C) DSC thermograms of the exothermic crystallization of 12HSA molecule gels.The diffractrograms from bottom to the top are butylnitrile, hexanenitrile, heptylnitrile.

D) DSC thermograms of the endothermic melting transition of 12HSA molecule gels. The diffractrograms from bottom to the top are butylnitrile, hexanenitrile, heptylnitrile.

E) DSC thermograms of the exothermic crystallization of 12HSA molecule gels. The diffractrogram is dodecylaldehyde

F) DSC thermograms of the endothermic melting transition of 12HSA molecule gels. The diffractrogram is dodecylaldehyde

G) DSC thermograms of the exothermic crystallization of 12HSA molecule gels.The diffractrograms from bottom to the top are 5-nonanone, 6-undecanone

H) DSC thermograms of the endothermic melting transition of 12HSA moleculegels. The diffractrogram from bottom to the top are 5-nonanone, 6-undecanone.

Appendix 3

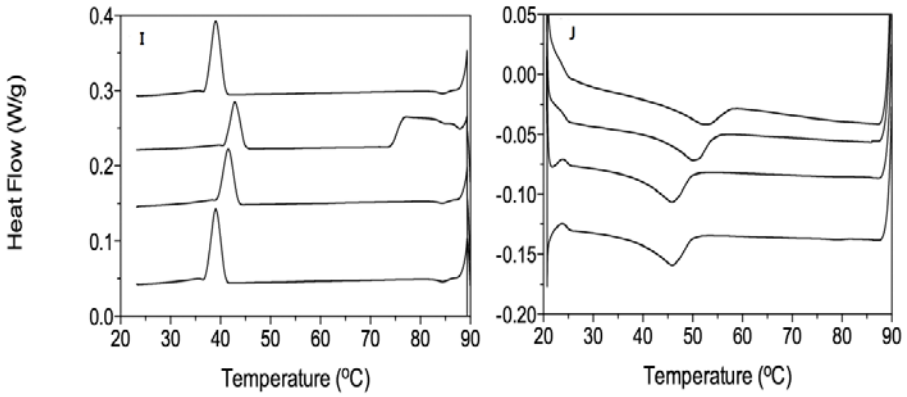

I) DSC thermograms of the exothermic crystallization of 12HSA molecule gels. The diffractrograms from bottom to the top are 1-hexanethiol, 1-heptanethiol, 1-octanethiol, 1-decanethiol.

J) DSC thermograms of the endothermic melting transition of 12HSA molecule gels. The diffractrogram from bottom to the top are 1-hexanethiol, 1-heptanethiol, 1-octanethiol, 1-decanethiol.

Appendix 4

HSPs, CGC and opacity of organogel in different organic solvent

Organic Solvent	ε_r	δ_T	δ_d	δ_p	δ_h	R_{ij}	CGC	State
	Unitless	$MPa^{1/2}$	$MPa^{1/2}$	$MPa^{1/2}$	$MPa^{1/2}$	$MPa^{1/2}$	WT%	
Pentane	1.82	14.90	14.90	0.00	0.00	9.11	0.5	Clear
Hexane	1.89	14.90	15.30	0.00	0.00	9.11	0.4	Clear
Heptane	1.91	15.30	15.50	0.00	0.00	8.66	0.3	Clear
Octane	1.95	15.50	15.70	0.00	0.00	8.45	0.3	Clear
Nonane	1.99	15.70	15.70	0.00	0.00	8.26	0.25	Clear
Decane	2.00	15.70	16.00	0.00	0.00	8.26	0.2	Clear
Dodecane	2.04	16.00	16.20	0.00	0.00	8.01	0.2	Clear
Tetradecane	2.06	16.20	16.40	0.00	1.80	7.86	0.5	Clear
Cyclopentane	1.96	16.50	16.80	0.00	0.20	6.21	0.5	Clear
Cyclohexane	2.01	16.80	17.50	0.00	0.00	7.34	0.4	Clear
Cyclooctane	2.11	17.50	17.70	0.00	0.00	7.35	0.4	Clear
Dichloromethane	8.51	20.23	17.80	3.10	5.70	3.69	2.5	Clear
Chloroform	4.81	18.94	18.20	6.30	6.20	1.17	N/A	No Gel
CCl_4	2.24	19.64	17.80	8.30	0.60	8.23	0.4	Clear
Octanal	8.60	17.75	16.10	5.80	4.70	4.67	2.8	Opaque
Nonanal	7.60	17.62	16.20	5.28	4.50	4.33	2.5	Opaque
Decanal	6.80	17.53	16.30	4.80	4.30	4.06	1.6	Opaque
2-Propone	17.00	19.94	15.50	10.40	7.00	2.65	N/A	No Gel
3-Pentone	11.20	18.15	15.80	7.60	4.70	2.17	N/A	No Gel
4-Heptone	10.60	17.50	15.80	5.70	4.90	2.21	N/A	No Gel
5-Nonanone	8.30	17.25	16.00	4.70	4.40	2.10	2.1	Clear
6-Undecanone	8.00	17.21	16.10	4.40	4.20	2.05	1.6	Clear
Diethyl ether	4.33	15.64	14.50	2.90	5.10	6.40	N/A	No Gel
Dipropyl ether	3.34	16.10	15.10	4.20	3.70	6.00	2.2	Clear
Dibutyl ether	3.22	16.13	15.20	3.40	4.20	5.45	1.5	Clear
Dipentyl ether	3.10	16.00	15.30	3.30	4.40	5.30	1.4	Clear
Ethanenitrile	37.50	24.40	15.30	18.00	6.10	15.83	2.3	Opaque
Propanenitrile	27.20	21.65	15.30	14.30	5.50	12.39	2.3	Opaque
Butanenitrile	20.30	20.40	15.30	12.50	5.10	10.80	2.1	Clear
Hexanenitrile	17.26	18.56	15.30	9.50	4.50	8.38	1.9	Clear
Octanenitrile	14.70	17.56	15.30	7.60	4.10	7.11	1.5	Clear
Nonanenitrile	14.00	17.00	15.30	6.60	3.80	6.62	0.9	Clear
1-Butanol	17.92	23.20	16.00	5.70	15.80	3.97	N/A	No Gel
1-Pentanol	14.50	21.93	15.90	5.90	13.90	3.73	N/A	No Gel
1-Hexanol	13.02	21.04	15.90	5.80	12.50	3.54	N/A	No Gel
1-Heptanol	11.48	20.52	16.00	5.30	11.70	3.42	N/A	No Gel
1-Octanol	9.75	21.01	17.00	3.30	11.90	3.45	N/A	No Gel
1-Nonanol	8.58	20.44	16.80	4.80	10.60	3.26	N/A	No Gel
1-Decanol	7.70	19.44	16.00	4.70	10.00	3.16	N/A	No Gel
1-Propanoic acid	3.20	19.95	14.70	5.30	12.40	8.43	N/A	No Gel
1-Butanoic acid	2.88	19.11	14.80	5.00	11.00	7.32	N/A	No Gel
1-Pentanoic acid	2.66	18.65	15.00	4.10	10.30	6.39	N/A	No Gel
1-Hexanoic acid	2.82	18.17	15.00	4.10	9.40	5.94	N/A	No Gel
1-Heptanoic acid	3.03	18.48	15.80	3.80	8.80	4.22	N/A	No Gel
1-Octanoic acid	2.82	17.50	15.10	3.30	8.20	5.20	N/A	No Gel

1-Nonanoic acid	1.72	18.05	16.00	3.00	7.80	3.35	N/A	No Gel
1-Pentanethiol	4.67	17.45	16.30	4.60	4.20	2.05	0.5	Clear
1-Hexanethiol	4.34	17.25	16.30	4.10	3.90	1.97	0.45	Clear
1-Heptanethiol	4.11	17.17	16.35	3.70	3.70	1.92	0.45	Clear
1-Octanethiol	3.95	17.09	16.40	3.30	3.50	1.87	0.4	Clear
1-Decanethiol	3.84	17.02	16.45	2.90	3.30	1.80	0.3	Clear
1-Butanamine	4.90	17.78	14.95	4.50	8.50	2.92	N/A	No Gel
1-Pentanamine	5.36	17.56	15.20	3.87	7.90	2.81	N/A	No Gel
1-Hexanamine	3.53	17.46	15.40	3.40	7.50	2.74	N/A	No Gel
1-Heptylamine	3.42	17.42	15.50	3.10	7.30	2.70	N/A	No Gel
1-Octanamine	3.30	17.37	15.60	2.80	7.10	2.66	N/A	No Gel